NASA TECHNICAL NOTE

NASA TN D-7573

NASA TN D-7573

PERFORMANCE OF A FLIGHT-TYPE LAMINAR RADIATOR WITH A BRAYTON POWER SYSTEM

by Theodore C. Cintula, George M. Prok, and Robert B. Smith

Lewis Research Center
Cleveland, Ohio 44135

NATIONAL AERONAUTICS AND SPACE ADMINISTRATION • WASHINGTON, D. C. • MARCH 1974

1. Report No.	2. Government Accession No.	3. Recipient's Catalog No.
NASA TN D-7573		

4. Title and Subtitle	5. Report Date
PERFORMANCE OF A FLIGHT-TYPE LAMINAR RADIATOR WITH A BRAYTON POWER SYSTEM	MARCH 1974
	6. Performing Organization Code
7. Author(s)	8. Performing Organization Report No.
Theodore C. Cintula, George M. Prok, and Robert B. Smith	E-7716
	10. Work Unit No.
9. Performing Organization Name and Address	502-25
Lewis Research Center National Aeronautics and Space Administration Cleveland, Ohio 44135	11. Contract or Grant No.
	13. Type of Report and Period Covered
12. Sponsoring Agency Name and Address	Technical Note
National Aeronautics and Space Administration Washington, D.C. 20546	14. Sponsoring Agency Code

15. Supplementary Notes

16. Abstract

A space-type laminar-flow radiator was designed and integrated with a 2- to 15-kilowatt Brayton electrical power generating system. The design, fabrication, and testing of this radiator are presented. Test results include performance under steady-state and transient conditions. Included in the transient results is performance in a simulated low earth orbit. Results show that the computer design is conservative. Orbital transients show that a further reduction in radiator area over that determined from steady-state conditions is possible. Radiator efficiency was always greater than 83 percent.

17. Key Words (Suggested by Author(s))

Space power
Brayton engine
Radiator
Heat transfer
Laminar flow

18. Distribution Statement

Unclassified - unlimited

Cat. 03

19. Security Classif. (of this report)	20. Security Classif. (of this page)	21. No. of Pages	22. Price*
Unclassified	Unclassified	47	$3.00

* For sale by the National Technical Information Service, Springfield, Virginia 22151

PERFORMANCE OF A FLIGHT-TYPE LAMINAR RADIATOR WITH A BRAYTON POWER SYSTEM

by Theodore C. Cintula, George M. Prok, and Robert B. Smith

Lewis Research Center

SUMMARY

A space-type laminar-flow radiator was designed and integrated with a 2- to 15-kilowatt Brayton electrical power generating system. The radiator is dimensionally compatible with existing spacecraft and is armored with redundant flow channels for meteoroid protection. Flow passages in the radiator are D-shaped because the radiator operated in the laminar-flow regime. The design, fabrication, and testing of this radiator are presented. Testing was done in a simulated space environment. The effective heat-sink temperature ranged from 250 to 195 K (-10° to -110° F).

Steady-state radiator performance was entirely satisfactory to the Brayton engine, and all test parameters were successfully achieved. Radiator performance was 83 percent or greater. Results show that the computer design is conservative.

Transient performance included the effect of varying both the engine parameters and the effective heat-sink temperature. Orbital transients were obtained by varying the heat-sink temperature as a function of time. The step changes from sun to shade and shade to sun were accomplished with an array of quartz lamps shining on one side of the radiator. The orbital transients show that a further reduction in radiator area over that determined from steady-state conditions is possible. For all orbital transients, a repeating cycle occurred by the fourth orbit.

INTRODUCTION

The Lewis Research Center has developed and tested a Brayton-cycle powerplant with the ultimate intent of providing a compact electrical power system for extended space missions (refs. 1 to 5). Over 2500 hours of successful operation have been accumulated on a Brayton-cycle power system. This testing was done in the vacuum environment of the Space Power Facility at Plum Brook Station (refs. 1 and 2). The first

part of the test program used an electric heat source in place of an isotope or nuclear heat source and a facility heat exchanger for waste-heat rejection. For the second part of the test program, a space-type radiator was designed and integrated with the Brayton engine (ref. 6). This report presents the conceptual logic for a space radiator as the medium of heat rejection, including the development and final design configuration of the radiator. The emphasis of this report is, however on the steady-state and transient performance of the radiator in combined systems testing.

All measurements reported herein were made in the U.S. customary system of units. Conversion to the International System of Units (SI) was done for reporting purposes only.

SYMBOLS

f	flow passage friction factor, 16/Re (for laminar flow)
Re	Reynolds number
T	temperature, K; ^{o}F
ΔT_{film}	temperature differential between bulk fluid and radiator tube surface, K; ^{o}F
ΔT_{fin}	temperature differential between radiator tube surface and mid-fin surface, K; ^{o}F
α	surface absorptivity, 0.22
ϵ	surface hemispherical emittance, 0.93

RADIATOR DESIGN

The testing of the 2- to 15-kilowatt Brayton system with a facility waste-heat exchanger verified the coolant requirements for the Brayton components. A radiator design point based on Brayton operating conditions is shown in figure 1 and table I. The Brayton coolant pump was designed to circulate a silicone oil with a viscosity of 2×10^{-6} m^2/sec (2 cS) at 298 K (77^{o} F). The qualifications of this operating fluid for the waste-heat-rejection system in a space mission were

(1) A viscosity curve that is flat with temperature

(2) A pour point of 173 K (-148^{o} F) (i.e., will not freeze in a near earth orbit)

(3) Constant fluid properties over the anticipated lifetime

The physical properties of the silicone oil were compatible for both Brayton cooling and

space orientation; therefore, a second medium was not considered. In addition, the Brayton system coolant restricted the waste-heat-rejection system to a pressure drop of 200 kN/m^2 (30 psid).

For the radiator to dissipate 17.6 kilowatts of heat at an operating range of 414 to 295 K (286° to 71° F) and rejecting to a 250 K (-10° F) sink, a minimum realistic area greater than 41.9 square meters (450 ft^2) was required. This area could be transformed into a practical configuration by sizing the radiator to conform to the outer skin of a typical spacecraft, 6.6 meters (21.7 ft) in diameter.

The total coolant flow rate was 0.164 kg/sec (1.36 lbm/sec). Capillary-size tubes are required to achieve turbulent flow from the low total flow. Since each tube must be armored for a given meteoroid protection, the requirement for many armored capillary tubes imposed a severe weight penalty.

The alternative was a laminar-flow radiator. In this flow regime, tubes of relatively large cross section could be used with acceptable fin spacing. Laminar flow satisfied the physical requirements of the radiator. Its efficiency as a heat-rejection mode has been demonstrated in nonround tubes (ref. 7). Therefore, from reference 7, a seemingly favorable option was to increase the tube perimeter for a given cross-sectional area. This would increase heat rejection in direct proportion to the increased wetted tube perimeter.

The general intent was to design a space radiator to be as practical and inexpensive as possible while improving the state of the art. The specific design requirements were that the radiator be

(1) Dimensionally useful to space applications

(2) Constructed of conventional materials by conventional techniques

(3) As light as possible (flight weight)

(4) Able to fullfill flight requirements

  (a) Meteoroid protection

  (b) Welded tube fittings

  (c) Emissive coating with $\alpha/\epsilon \sim 0.20$

  (d) Redundant heat-rejection passages

  (e) Five-year mission

An operating radiator with these design requirements is unknown. The problems are as follows:

(1) Can the radiator be efficient?

(2) Can a theoretical analysis of the radiator be substantiated?

(3) What are the effects of operating the radiator at other than the design point?

The radiator analysis was performed by using a computer program. This program was originally developed for the conceptual analysis of a laminar-flow space radiator with internal fins (refs. 8 and 9). The program was modified for external-fin heat

transfer, the specified silicone fluid, and variations in tube geometry (ref. 6). In its final form the program could determine a minimum-weight radiator with armored tubing for a specified meteoroid protection. For practicality, the computer design was restricted to using commercially available panel thicknesses, uniform tube cross sections, and the same number of tubes per radiator panel for both the low-temperature and high-temperature radiator panels.

To supplement the analytical radiator design, a small-scale-radiator test program was performed at the Space Power Facility (ref. 7). The small-scale program was specifically oriented to provide information on low-temperature laminar-flow radiative heat transfer that would be directly applicable to the full-scale radiator. The prominent results of the small-scale tests were the following:

(1) Low-temperature heat transfer resulted in a small temperature differential between the bulk fluid and the tube surface, despite the low thermal conductivity of the fluid, 0.1 W/m-K (0.06 Btu/hr-ft-^{o}F).

(2) Heat transfer and pressure drop for an elongated-tube cross section could be predicted with accuracy.

(3) In laminar flow, low-temperature heat transfer was relatively independent of Reynolds number.

Also, the small-scale program provided actual test data for reliable estimates of the heat-tranfer and pressure-drop correlations of the computer program.

A schematic of the system for the computer-designed radiator is shown in figure 2. The total radiator area was divided into two segments, a high-temperature radiator supplied solely by the discharge of the Brayton waste-heat exchanger and a low-temperature radiator which handles the entire coolant flow. The dual radiators saved approximately 15 percent in total area from a single radiator concept. The computer design specified an elongated-tube geometry, the fin spacings, and the armor thickness for the mission. The high-temperature radiator had an area of 26.4 square meters (284 ft^2) to reject 12.1 kilowatts of waste heat. The low-temperature radiator had an area of 27.1 square meters (292 ft^2) to reject the remaining 5.5 kilowatts of heat. The computer design analysis specified redundant radiator flow channels in each radiator, based upon a minimum-weight armored tubing configuration. The primary flow channels are designated "loop A," and the redundant channels "loop B."

The tube geometry used in the computations and the resultant tube designs are shown in table II. An arithmetical average of the actual internal tube dimensions is given in table III. The low-temperature-radiator tube was larger than the high-temperature-radiator tube. This was necessary because the low-temperature radiator circulates the entire coolant.

There were six active and six redundant tubes in each high- and low-temperature-radiator panel. The distance between active tubes on each radiator was 12.5 centimeters

(5 in.), the fin thickness for each radiator was 0.076 centimeter (0.030 in.), and the armor thickness was 0.63 centimeter (0.25 in.). Both radiators were fabricated from identical stock thicknesses. Their different tube geometries had slightly different no-puncture probabilities for their 5-year mission (ref. 10). The entire radiator as a space package had an overall no-puncture probability of 0.99 for a 5-year mission.

RADIATOR FABRICATION AND INSTALLATION

It was decided to form the radiator tube, armor, and fin from a diffusion-bonding process used commercially in refrigeration systems and also used as the radiator panel in the small-scale tests (ref. 7). The Apollo radiators used this concept.

In the diffusion-bonding process, panels are made by sandwiching, at the tube and manifold locations, stopweld material between two sheets of aluminum. A diffusion bond welds the aluminum sheets together except where stopweld exists. Tubes and manifolds are formed by pressurizing the stopwelds to separate the two pieces of aluminum. Inflation height is accurately controlled by a fixed plate. The final radiator panel geometry was obtained by having one sheet of aluminum equal to armor thickness, 0.56 centimeter (0.220 in.), and the other equal to fin thickness, 0.076 centimeter (0.030 in.). Stopwelds were also located at nonarmored radiator fin areas (fig. 3). A mill cut at the armor edges allowed the excess armor to be removed.

The maximum panel manufacturing dimensions were approximately 2.7 meters (9 ft) by 0.9 meter (3 ft). Allowing for trim and excess, each of the high- and low-temperature radiators would consist of 16 panels. The most satisfactory panel arrangement was the high-temperature radiator on the bottom and the low-temperature radiator on the top, as shown in figure 4. Both high- and low-temperature radiators were two panels high (fig. 4(a)). The high-temperature fluid inlet was at the center of the radiator, where the flow was split between the various segments of panels. Each segment was four panels long. The low-temperature fluid was split in the same manner. However, it was mixed with the fluid from the high-temperature radiator before it entered the low-temperature radiator (fig. 4(b)). The flows were recombined at the radiator discharge.

After each panel was rolled to the proper diameter, the 0.74-meter (2.5-ft) high panels were joined edgewise by welding at the radiator fin to ensure thermal integrity. The double-height dual radiator panels were joined lengthwise by removing the abutting manifolds, shown in figure 5, from each dual panel and by butt welding respective tubes, fins, and armor together. Prior to welding, the radiator tubes were expanded (fig. 5(a)), and aluminum chill rings were installed to prevent possible tube restriction by the weld process. This procedure was followed to form eight segments each two panels long by two panels high. Segments were formed into the final radiator configuration by connect-

ing adjacent panel headers with round tubing (figs. 4 and 5). This permitted insertion of a mid-radiator fluid-temperature probe.

Radiator headers were formed from 2.2-centimeter (7/8-in.) outside diameter rods cut lengthwise and hollowed out to a 1.2-centimeter (1/2-in.) inside diameter. The headers were welded to the radiator panels (fig. 5(b)). Redundancy was maintained by dual headers on one end of each panel. Flow was distributed from the headers to individual tubes by 0.6-centimeter (1/4-in.) diameter drilled hole passages into the expanded tube section. The manifold inlet to the headers was 1-centimeter (3/8-in.) diameter schedule 40 pipe.

The entire radiator configuration as tested is shown in figure 4(a). The radiator was mounted from a 6.6-meter (21.7-ft) diameter support. The low-temperature radiator was suspended from the circular support structure by extension springs. The high-temperature radiator was supported from the low-temperature radiator by a stainless-steel circumferential band. The band was slotted lengthwise to allow thermal expansion, and each radiator was thermally insulated from the band. Otherwise, the radiators were not in contact with the support structure.

The temperatures shown in figure 4(a) are design fluid temperatures measured at the manifolds. High-temperature flow, 414 K (286° F), from the Brayton waste-heat exchanger was circulated through the high-temperature radiator. At the high-temperature-radiator discharge, the fluid had cooled to the low-temperature-radiator inlet temperature (314 K (105° F), the discharge temperature of the combined flow of the Brayton rotating unit and the cold plates). The high-temperature flow was combined with flow from these components at the low-temperature inlet manifolds. The fluid was cooled to 295 K (71° F) at the low-temperature discharges. As power levels of the Brayton engine are varied, coolant temperatures and consequently total heat rejection will change (ref. 1). To compensate partially for severe off-design operation, and as a variable for studying radiator performance, a remotely operated bypass valve was installed parallel to the high-temperature radiator (figs. 4(b) and 6). This valve permitted a portion of the high-temperature coolant to flow directly into the low-temperature-radiator manifold inlet. The effect is to study the performance of a fixed-area radiator acting as a variable-area radiator.

The radiator as installed at the Space Power Facility test chamber is shown in figures 7 and 8. The vacuum chamber is 30.5 meters (100 ft) in diameter by 37 meters (122 ft) high. It is capable of continuous operation in the 10^{-7}-torr range. The radiator was centrally located in a cold wall 12 meters (40 ft) in diameter by 12 meters (40 ft) high and directly above the Brayton power system.

The radiator was coated with a white high-emissivity (ϵ = 0.93), low-absorptance (α = 0.22) paint. The inner circumference of the entire radiator was shielded with a multilayer insulation blanket. Thus, radiative heat transfer was permitted from the white surface (armored) side of the radiator only.

The cold wall's interior was coated with a black paint. This surface was a good absorber of incident radiation in all wavelengths. The cold wall's temperature was maintained by circulating chilled gaseous nitrogen. The cold wall's operating range was at least from 250 to 195 K (-10° to -110° F), which represents the sun-shade temperature extremes of a low earth orbit. These effective heat-sink temperatures were determined by the α/ϵ of the radiator coating. The cold wall circumferentially enclosed the radiator.

Eight calorimeters were located on the radiator's circumferential periphery. The temperature measured by each calorimeter was the effective heat-sink temperature to which the radiator dissipated heat. The radiator predominantly "saw" the cold wall. However, it was also exposed to the chamber floor and dome. The calorimeters are insulated devices, coated identically to the radiator, whose temperature is solely determined by incident absorbed radiation. Thus, the true average heat-sink temperature seen by the radiator was the average temperature of the calorimeters.

The lamp array shown in figure 8 was used in simulating an effective heat-sink temperature for sun-shade orbital transients. The effective heat-sink temperature for a 96-minute low earth orbit ($\sim$550 km) is shown in figure 9. For the orbital transients, the cold wall was at an effective heat-sink temperature of 195 K (-110° F). At full lamp power, the Brayton engine operated as if the cold wall was at 250 K (-10° F). The maximum power to the lamp array was determined experimentally. Power was supplied to the lamp array for the orbital test automatically by a preprogrammed power supply to give the effective heat-sink temperature shown in figure 9.

RESULTS AND DISCUSSION

Steady-State Performance

Brayton engine performance was mapped over a variety of steady-state test points. For each Brayton engine test point, data on radiator performance were obtained. Radiator surface thermocouples and flowmeter locations are shown in figure 4(b). Thermocouples for fluid temperatures were located at the inlet and outlet manifolds and in the header crossover tubing. From figure 4(b) it can be seen that only half of the high- and low-temperature radiators is well instrumented. For this reason, much of the analysis will be for only half of the total radiator area.

A steady-state temperature profile of both the high- and low-temperature-radiator segments is shown in figure 10. This figure is representative of the temperature design point of the radiators. The upper two curves are the fluid and tube-surface temperature profiles of the high-temperature radiator. The lower pair of curves are the respective fluid and tube-surface temperature profiles of the low-temperature radiator.

The difference between the fluid temperature and the tube-surface temperature is the film temperature drop ΔT_{film}. From figure 10, the film temperature drop continually decreases with decreasing fluid temperature. A representative average value was determined at the effective fluid temperature of each radiator.

A tube-fin temperature rake was located near the high-temperature-radiator inlet. The mid-fin temperature is shown in figure 10. Comparing temperature losses at this point substantiates that radiator performance is predominantly influenced by film losses rather than by fin losses.

Radiator heat dissipation was determined by loss of sensible heat of the fluid. While these curves closely represent the temperature design point, each radiator's flow was higher than the design point. Thus, the total heat-rejection rate was greater than the design condition. Each radiator was oversize. At the test conditions shown in figure 10, the high- and low-temperature radiators are 84.2 and 90.7 percent efficient, respectively. Radiator efficiency is determined from both film and fin temperature losses.

To make the radiator perform like a variable-area radiator, a remotely controlled valve was placed in a line bypassing the high-temperature radiator. The ratio of the flow of hot fluid bypassing the high-temperature radiator to the total flow of high-temperature fluid is the bypass ratio. Operation with approximately 35 percent high-temperature-radiator bypass flow is shown in figure 11. The predominant effect is a decreased fluid discharge temperature, which results in reduced heat-rejection rate. Despite the drastic reduction in Reynolds number from that shown in figure 10, ΔT_{film} is relatively unchanged. This suggests this parameter is predominantly influenced by temperature as reported in the small-scale tests (ref. 7). For this particular study, high- and low-temperature-radiator efficiencies were 81.9 and 90.1 percent, respectively.

Steady-state ΔT_{film} over the radiators' temperature range is shown in figure 12. The curve fit is approximately 36 percent higher than that obtained in the small-scale tests. This fit can be explained by the fact that the small-scale tests were performed in such an exacting fashion that optimal values of ΔT_{film} may have been obtained. Also, this parameter was directly measured in the small-scale tests and indirectly calculated in the full-scale radiator. However, since this parameter was small in magnitude, the percentage change produced no great bias in overall radiator efficiency. Low-temperature laminar-flow radiation still resulted in low ΔT_{film}. Higher temperature operation did result in an apparent drift from the normalizing curve. This again may be solely in the data-gathering techniques.

As ΔT_{film} was increased during the small-scale tests (ref. 7), the heat-transfer coefficient decreased proportionally, as shown in figure 13. The low-temperature-radiator heat-transfer coefficient closely correlated to the expected 36 percent decreases. The high-temperature-radiator heat-transfer coefficient more closely approximated the small-scale-test results.

The mid-fin temperature drop is shown in figure 14. Although these data were taken near the high-temperature-radiator inlet, the operating temperature range is applicable to realized temperatures of both the high- and low-temperature radiators. As previously mentioned, the parameter is less than film temperature losses for equivalent temperatures.

The laminar-flow friction factor for the low-temperature radiator closely correlated to the small-scale results given in reference 7, as shown in figure 15. These data combined with the small-scale-test results confirm that established pressure-drop predictions for extreme tube shapes in laminar flow can be determined accurately.

A radiator efficiency curve plotted against total fixed-area heat rejection when the radiator is operating at a 250 K (-10° F) sink is shown in figure 16. This curve was derived by choosing a fluid temperature and subtracting the corresponding film losses from figure 12 and half the fin losses from figure 14. The result is the effective radiator temperature at an effective fluid temperature. Total heat rejected was determined from the total radiator area rejecting at effective radiator temperature. Prime heat rejection was determined by the radiator fixed area with the radiator operating at the effective fluid temperature. The ratio of these terms multiplied by 100 percent is the radiator efficiency - actual heat rejected divided by maximum possible heat rejected from a given area. By using the graphical data it was possible to tabulate information beyond the heat-rejection rates actually tested.

The resulting curve illustrates the high efficiencies realized with low-temperature laminar-flow heat rejection. The actual test range for the high-temperature radiator was from 83.3 to 90.3 percent efficiency. The low-temperature radiator was from 84.0 to 90.8 percent efficient. Radiator design efficiencies were 84.0 and 88.2 percent, respectively.

The conjecture of forcing ever increasing heat-rejection rate from a fixed-area radiator is implied from figure 16. The available data indicate this additional load results in only minor efficiency losses and an absolute minimal efficiency of 83 percent. In retrospect, a minimal efficiency of 82.3 percent was achieved in the small-scale testing at the high-fluid-temperature, low-Reynolds-number test point. The implications of high minimal efficiencies associated with laminar-flow low-temperature heat transfer are not straightforward, but it does show promise even at elevated heat-rejection rates.

Constant Heat-Rejection Rate at Steady State

For a given sink temperature, the operation of the Brayton engine at set turbine inlet temperatures and compressor discharge pressures gave nearly constant heat-rejection rates. The radiator operating conditions to reject this constant heat flux are

shown in figure 17. This parameter was plotted for constant high- and low-temperature-radiator flow rates. The effect of decreasing heat-sink temperatures was reduced radiator operating temperatures. This decrease was approximately 1-degree reduction in operating temperature for each 4-degree decrease in sink temperature. The difference between radiator inlet and discharge temperatures was unchanged except for the minor variation in the specific-heat capacity of the fluid.

The effect of varying radiator flow conditions is shown in figure 18. Total radiator heat rejection, high- plus low-temperature radiators, was constant. The effect of increased flow rates was to decrease the ΔT between the radiator inlet and discharge temperatures. This decrease was most predominant at elevated fluid temperatures associated with the high-temperature-radiator inlet. Operation at a 195 K (-110° F) sink resulted in a nearly identical suppressed temperature range curve.

Steady-state Brayton coolant requirements could also be maintained at various heat-sink temperatures by bypassing a portion of the high-temperature-radiator coolant. In this case, identical Brayton component inlet and outlet temperatures and flow rates were preserved rather than component heat-rejection rates (fig. 18). Essentially, as heat-sink temperature was reduced, identical Brayton operating points were maintained by bypassing a portion of the high-temperature flow. This resulted in decreased high-temperature heat rejection and an accompanying increase in low-temperature-radiator heat-rejection rate. However, the total heat rejected did not change because the engine operating conditions were not changed. At a heat-sink temperature of 195 K (-110° F), about a 65-percent bypass of high-temperature fluid around the high-temperature radiator was required to maintain constant engine operating conditions.

Comparison of Design with Steady-State Results

To establish the accuracy of the radiator design computer program, actual test data were used as computer input. The program was modified for all actual physical differences between the designed radiator and the actual radiator. Fluid inlet and outlet temperatures and actual heat rejected were computer input parameters. From this information, the computer program predicted a radiator area. This area for nine conditions is given in table IV. The computer predictions average 18 percent higher than actual radiator area. This is in agreement with figure 10, where the condition of an oversize radiator was first realized, and with figure 16, where increased heat-rejection rates could occur with only minor decreases in efficiency.

To meet test objectives, it is good practice to design an oversize radiator. Consequently, the computer program must have built-in conservatism for such parameters as ΔT_{film} and ΔT_{fin}. This is apparent from the test program as the actual full-scale

ΔT_{film} was not as low as the small-scale-test results. If the Brayton radiators were in actuality undersize, certain Brayton test conditions could not be achieved.

From actual Brayton performance, the radiators performed satisfactorily and the degree of oversize produced no complications in achieving the test objectives. Therefore, the computer program predicted satisfactory performance for each area with a safe degree of conservatism. The computer results given in table IV also show that the Brayton radiator tends to be self-compensating toward the design point. Variations in inlet temperatures, flow rates, or tube restrictions had little effect on the total predicted area.

Transient Performance

In addition to cooling the Brayton alternator and electronics, the Brayton engine has four different heat exchangers (ref. 5). They include the heat source, the recuperator (a gas-to-gas heat exchanger), the waste-heat exchanger (a gas-to-liquid heat exchanger), and the radiator. Any change in the heat transfer of one of these heat exchangers will ultimately affect the performance of other engine components. Hence, the transient behavior of the radiator can be observed by

(1) A step change of the silicone oil flow rate in the waste-heat exchanger

(2) A step change in the compressor discharge pressure of the Brayton engine

(3) A change in the turbine inlet temperature

(4) A step change in the effective heat-sink temperature

(5) A change in the active coolant loop of the radiator from the "A" loop to the "B" loop

(6) A time-varying heat-sink temperature which simulates that of low earth orbit

A slight change of 12.5 percent (0.00456 to 0.00397 m^3/min, or 1.20 to 1.05 gal/min) in the silicone oil flow through the waste-heat exchanger and the high-temperature radiator shows up as a small but real transient in the radiator parameters (fig. 19). For the case shown in figure 19, the heat rejected by the radiator increased by about 0.5 kilowatt within 10 minutes after the start of the transient (fig. 19(a)). In the first 16 minutes, the temperature of the fluid to the high-temperature radiator increased a few degrees (fig. 19(b)). This temperature then decreased over the next 1/2 hour to reach a steady-state temperature slightly less than that at the start of the transient. A similar but opposite trend was observed in the temperatures at the high-temperature-radiator (fig. 19(c)) and low-temperature-radiator (fig. 19(d)) fluid outlet. Although the trend in figure 19(d) is on a much expanded scale, it is real and was consistently observed. Some transient change was observed in the low-temperature-radiator fluid (fig. 19(c)), but it was small because only about 33 percent of the flow came from the

high-temperature radiator. Radiator transients were always observed when the silicone fluid flow through the waste-heat exchanger was changed. The only uncertainty was if the temperatures would rise and then fall, or if they would fall and then rise. This behavior is an engine parameter that depends on the coolant flow through the waste-heat exchanger. In any case, the entire transient condition reached steady-state in less than an hour.

The transient behavior of the radiator parameters following a change in the Brayton engine compressor discharge pressure is shown in figures 20 and 21. For increasing compressor discharge pressure, the transients increased as would be expected. A decrease in compressor discharge pressure produced a short-term and a long-term transient. The short-term transient occurred during the first 10 minutes (fig. 21(a)). The long-term transient took place over the next 60 to 90 minutes. A short-term transient did not occur in the radiator for the high-temperature-radiator inlet when the compressor discharge pressure was decreased (fig. 21(b)). In any case, it took about $1\frac{1}{2}$ hours for steady-state to be reached after a change in compressor discharge pressure.

Figures 22 and 23 show the effect of the Brayton engine turbine inlet temperature transients on the various radiator parameters. During one of these transients, the turbine inlet temperature was increased from 1030 K (1400° F) to 1090 K (1500° F) at the rate of about 3 kelvins (5 deg F) per 5 minutes. The other temperature transient was a step change from 1090 K (1500° F) to 1100 K (1520° F). The discontinuities in figures 22(a) and 23(a) are the result of temperature readings that were affected by the controls for the Brayton engine electric heat source. Temperature readings that clearly exhibit this are in figure 22(d) (between 118 and 126 min) and figure 23(d) (between 62 and 76 min). When the turbine inlet temperature was gradually increased from 1030 K (1400° F) to 1090 K (1500° F), the radiator transients continued for about 1 hour after the final heat-source setting. An 11-kelvin (20-deg F) step increase in the controls for the electric heat source resulted in radiator transients that continued for about 2 hours until steady-state was reached (fig. 23). There were short-term and long-term transients of some radiator parameters for this temperature change (figs. 23(b) and (c)).

The radiator transients caused by step changes in heat-sink temperature from 256 K (0° F) to 195 K (-110° F) and from 195 K (-110° F) to 256 K (0° F) are shown in figures 24 and 25, respectively. These transients are essentially the worst-case sunshade transients. All these transients are basically long-term transients that take more than 3 hours to reach steady state. It was possible to obtain these transients by using the quartz lamp array (fig. 8) that was installed for the orbital transients.

The transient effect caused by a waste-heat-coolant pump failure was determined by turning the active loop pump off and the redundant one on. When the active pump was turned off and the redundant pump was simultaneously turned on, the radiator recovered to steady-state conditions in about 30 minutes. If there was a 4-minute lapse before the

redundant pump was turned on, it took more than 1 hour for steady-state conditions to be reached.

Radiator transients were measured with the Brayton engine operating in a simulated 96-minute low earth orbit. The effective heat-sink temperature shown in figure 9 was achieved by automatically programming the power to the quartz lamp array. The power supplied to the quartz lamps is shown for four orbits in figure 26. The cold wall was maintained at a heat-sink temperature of 195 K (-110° F) during these orbital transients. Examples of some high-temperature-radiator fluid inlet temperature transients and the radiator outlet temperature transients are shown in figures 27 and 28. Orbital transients were initiated with the engine operating at sun conditions (250 K (-10° F) heat-sink temperature). This was accomplished by bypassing about 65 percent of the waste-heat-exchanger fluid around the high-temperature radiator with the cold wall at a heat-sink temperature of 195 K (-110° F). After the steady state was reached, the bypass valve was closed and the orbital mode for the quartz-lamp-array power supply was started. The lone exception was the second case in the following listing, where the orbital mode was started from steady-state shade conditions (bypass valve closed). The five cases of engine operation were

(1) Constant gas inventory and constant heat-source power

(2) Constant gas inventory and constant turbine inlet temperature (the only case starting at steady-state engine operation under shade conditions)

(3) Constant gas inventory and constant turbine inlet temperature (fig. 27)

(4) Constant compressor discharge pressure and constant turbine inlet temperature

(5) Constant compressor discharge pressure and constant heat-source power (fig. 28)

The transients for cases 1 and 4 exhibited characteristic curves like that of case 3, with temperatures differing by only a few degrees at any orbital time. Although the transients for case 5 look similar to those of case 3, the temperatures are significantly different. The actual temperatures for these transients are tied to engine transients which are outside the scope of this report. The initial transient for fluid inlet temperature (figs. 27(a) and 28(a)) was a fluid flow transient caused by closing the bypass valve. A decrease of 7 percent in the silicone oil flow to the waste-heat exchanger occurred when the bypass valve was closed. The initial decrease in radiator outlet temperature (figs. 27(b) and 28(b)) occurred primarily because the entire radiator was used when the bypass valve was closed. When the bypass valve was not used, the starting point for case 2, the initial radiator outlet temperature transient was absent (fig. 29). For all orbital transients, a repeating cycle occurred by the fourth orbit. There was no lag in the radiator outlet temperature with respect to the power for the quartz lamp array going on or off (figs. 26, 27(b), 28(b), and 29). However, the radiator inlet temperature lagged the power on or off by about 5 minutes (figs. 26, 27(a), and 28(a)).

Of the two orbital transients, the radiator outlet is the more important one for the Brayton engine. By the fourth orbit, this temperature was 286 to 287 K (±4 kelvins) or 55° to 57° F (±7 deg F) depending on the Brayton engine operating mode. This is an average of 9 kelvins (16 deg F) below the steady-state operating point, which means the radiator is oversize for orbital conditions.

An average equivalent heat-sink temperature for low earth orbit might be a more desirable design parameter for the radiator. The long-term transients observed during simulated orbits are what should have been expected from the heat-sink-temperature transient in figures 24 and 25.

SUMMARY OF RESULTS AND CONCLUSIONS

A radiator was designed, fabricated, and tested with a 2- to 15-kilowatt Brayton power system. Both steady-state and transient results were obtained. The transient results included testing in a simulated low earth orbit. The major results include the following:

1. For steady-state conditions, the radiator was about 18 percent oversize. Thus, the computer program used in designing the radiator was conservative.

2. The low-temperature radiator operated at an efficiency of 84.0 to 90.8 percent, and the high-temperature radiator operated at an efficiency of 83.3 to 90.3 percent.

3. A low-temperature radiator with laminar flow can operate efficiently. An apparent lower limit on the efficiency is 83 percent.

4. A low-temperature laminar-flow radiator is self-compensating toward the design point.

5. After a step change in Brayton engine operating conditions, it will take 1 to 2 hours for steady-state to be reached.

6. After a step change in heat-sink temperature from shade to sun, it will take more than 3 hours for the radiator to reach steady state.

7. Orbital transients show that a repeating cycle is reached by the fourth orbit.

8. The Brayton radiator can be made smaller for operation in low earth orbit than the steady-state heat-sink conditions indicates.

9. There were no large variations in the behavior of the radiator under low-earth-orbit variations in heat-sink temperature. The radiator outlet temperature varied less than ±4 kelvin (±7 deg F) around the mean radiator outlet temperature.

10. A non-round-tube laminar-flow radiator does not add a significant weight penalty to a flight-type Brayton power conversion system.

Lewis Research Center,
National Aeronautics and Space Administration,
Cleveland, Ohio, November 21, 1973,
502-25.

REFERENCES

1. Fenn, David B.; Deyo, James N.; Miller, Thomas J.; and Vernon, Richard W.: Experimental Performance of a 2-15 Kilowatt Brayton Power System in the Space Power Facility Using Krypton. NASA TM X-52750, 1970.
2. Vernon, Richard W.; and Miller, Thomas J.: Experimental Performance of a 2-15 Kilowatt Brayton Power System Using a Mixture of Helium and Xenon. NASA TM X-52936, 1970.
3. Glassman, Arthur J.: Summary of Brayton Cycle Analytical Studies for Space-Power System Applications. NASA TN D-2487, 1964.
4. Wong, Robert Y.; Evans, Robert C.; Spackman, Donald J.; and Winzig, Charles H.: Injection Start of a Brayton Cycle Turbocompressor Operating on Gas Bearings in a Closed Loop. NASA TM X-1590, 1968.
5. Klann, John L.; and Hettel, Henry J.: Predictability of Brayton Electric Power System Performance. NASA TN D-6808, 1972.
6. Miller, Thomas J.; Couch, James P.; and Prok, George M.: Design and Preliminary Testing of a Brayton Space Radiator Concept. NASA TM X-2401, 1971.
7. Cintula, Theodore C.; Prok, George M.; and Johnston, Daniel B.: Laminar Flow Studies of a Low-Temperature Space Radiator Model Using D-Shaped Tubes. NASA TN D-6727, 1972.
8. Larson, John W.; and Couch, James P.: Comparison Between Vapor Chamber and Conducting Fin Brayton Radiators. Intersociety Energy Conversion Engineering Conference. Vol. 1. IEEE, 1968, pp. 416-426.
9. Gerrels, E. E.; and Larson, J. W.: Brayton Cycle Vapor Chamber (Heat Pipe) Radiator Study. NASA CR-1677, 1971.
10. Loeffler, I. J.; Lieblein, Seymour; and Clough, Nestor: Meteoroid Protection for Space Radiators. Power Systems for Space Flight, Vol. XI of Progress in Astronautics and Aeronautics, Morris A. Zipkin and Russel N. Edwards, eds., Academic Press, 1963, pp. 551-579.

TABLE I. - PROPOSED RADIATOR DESIGN-POINT

SPECIFICATIONS

Coolant flow rate, g/sec (lbm/sec)	164 (0.36)
Maximum pressure drop, kN/m^2 (psid)	200 (30)
Maximum possible inlet temperature, K (^oF)	414 (286)
Minimum possible outlet temperature, K (^oF)	295 (71)
Heat rejected, kW	17.6
Heat-sink temperature, K (^oF)	250 (-10)
Emissivity	0.93
Material	1100 Aluminum
Coolant	Silicone oil
Coolant viscosity at 298 K (77^o F), m^2/sec (cS)	2×10^{-6} (2)
Overall no-puncture probability	0.99
Mission time, yr	5

TABLE II. - RADIATOR EXPANDED-TUBE AND FIN DIMENSIONS

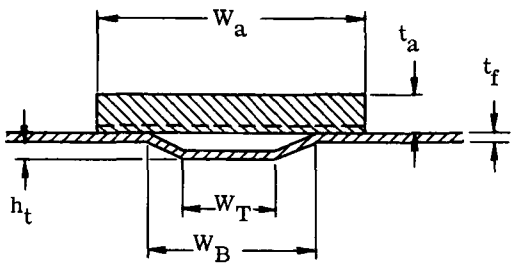

[No-puncture probability (5-yr lifetime for entire redundant tube radiator), 0.99.]

	High-temperature radiator	Low-temperature radiator
Tube bottom width, W_B, cm (in.)	0.965 (0.38)	1.778 (0.70)
Tube top width, W_T, cm (in.)	0.483 (0.19)	0.889 (0.35)
Tube height, h_t, cm (in.)	0.099 (0.039)	0.117 (0.046)
Fin thickness, t_f, cm (in.)	0.076 (0.03)	0.076 (0.03)
Armor thickness, t_a, cm (in.)	0.63 (0.25)	0.63 (0.25)
Armor width, W_a, cm (in.)	2.286 (0.90)	3.048 (1.20)
Number of active tubes	24	24
Number of redundant tubes	24	24
Distance between active tubes, cm (in.)	12.70 (5.0)	12.70 (5.0)
Radiator area, m^2 (ft^2)	26.4 (284)	27.1 (292)
Radiator mass, kg (lbm)	291 (643)	296 (653)

TABLE III. - INTERNAL TUBE DIMENSIONS - COMPOSITE

AVERAGE OF 12 TUBES

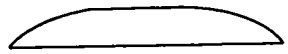

D-shaped tube

	High-temperature radiator	Low-temperature radiator
Base, cm (in.)	0.965 (0.38)	1.753 (0.69)
Flat top, cm (in.)	0.254 (0.10)	0.864 (0.34)
Height, cm (in.)	0.099 (0.039)	0.117 (0.046)
Perimeter, cm (in.)	1.961 (0.772)	3.548 (1.397)
Cross-sectional area, cm^2 ($in.^2$)	0.074 (0.0115)	0.178 (0.0276)
Hydraulic diameter, cm (in.)	0.151 (0.0596)	0.201 (0.0790)

TABLE IV. - FINAL COMPUTER RADIATOR-AREA PREDICTIONS

[Actual area, m^2 (ft^2): high-temperature radiator, 26.4 (284); low-temperature radiator, 27.1 (292).]

	Fluid inlet temperature		Fluid outlet temperature		Flow rate		Predicted area		Deviation, percent
	K	^oF	K	^oF	g/sec	lbm/sec	m^2	ft^2	
High-temperature radiator	126.7	260	31.7	89	68.0	0.15	31.4	338	19
	147.8	298	28.9	84	72.6	.16	32.0	344	21
	86.7	188	36.1	97	108.9	.24	30.9	333	17
	124.4	256	43.3	110	81.6	.18	31.3	337	19
Low-temperature radiator	45.0	113	23.9	75	186.0	0.41	32.5	350	20
	39.4	103	22.2	72	204.1	.45	31.3	337	15
	37.8	100	19.4	67	186.0	.41	32.0	345	18
	36.7	98	21.1	70	217.7	.48	31.4	338	16
	40.6	105	22.2	72	195.0	.43	31.5	339	16

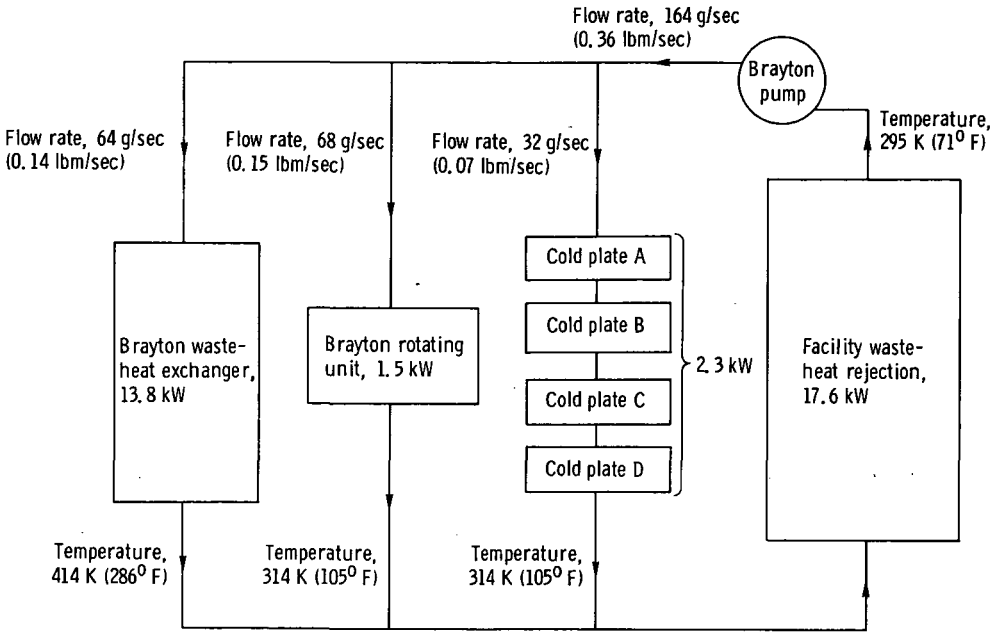

Figure 1. - Schematic of Brayton-cycle coolant loop - design point for proposed waste-heat-rejection system.

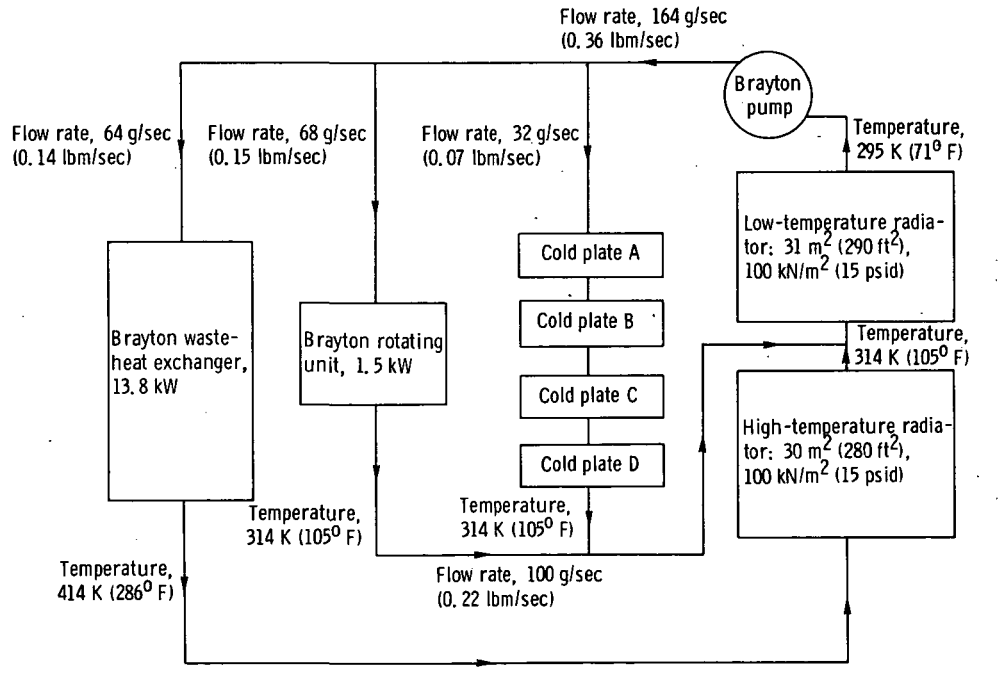

Figure 2. - Schematic of Brayton-cycle coolant loop - design point for space radiator heat-rejection system.

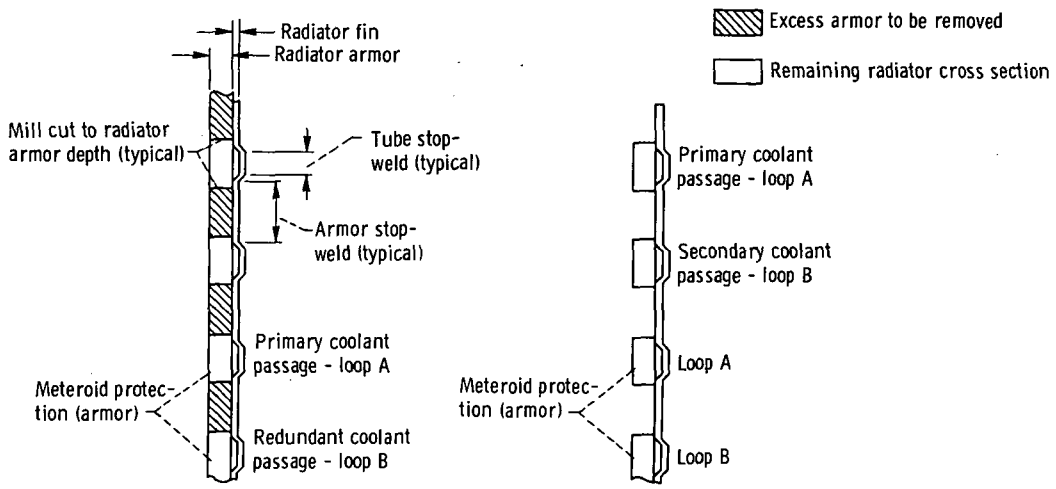

Figure 3. - Radiator cross section, showing areas of stopweld and mill cuts to achieve final configuration.

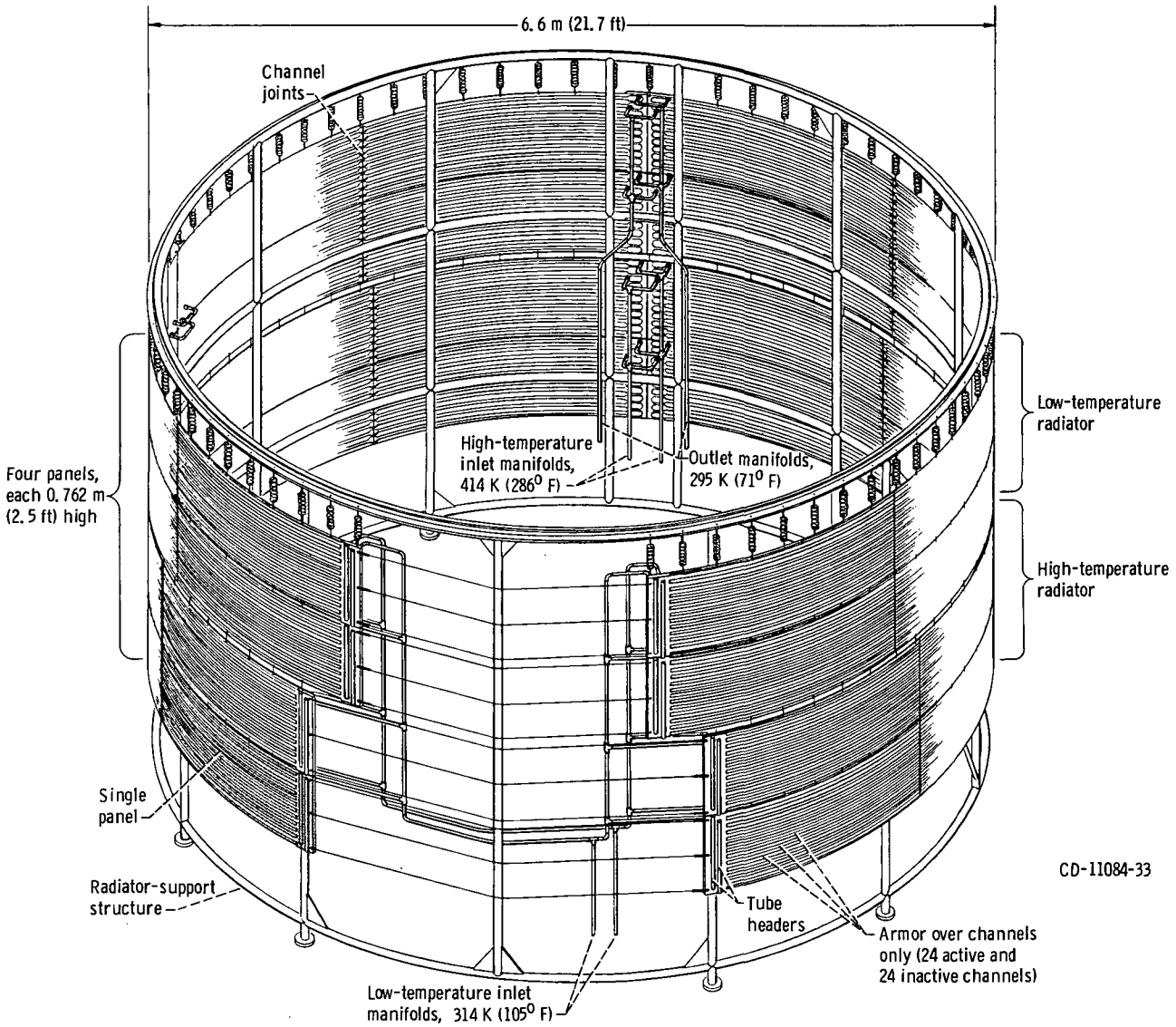

(a) Details of construction.

Figure 4. - Brayton-cycle radiator.

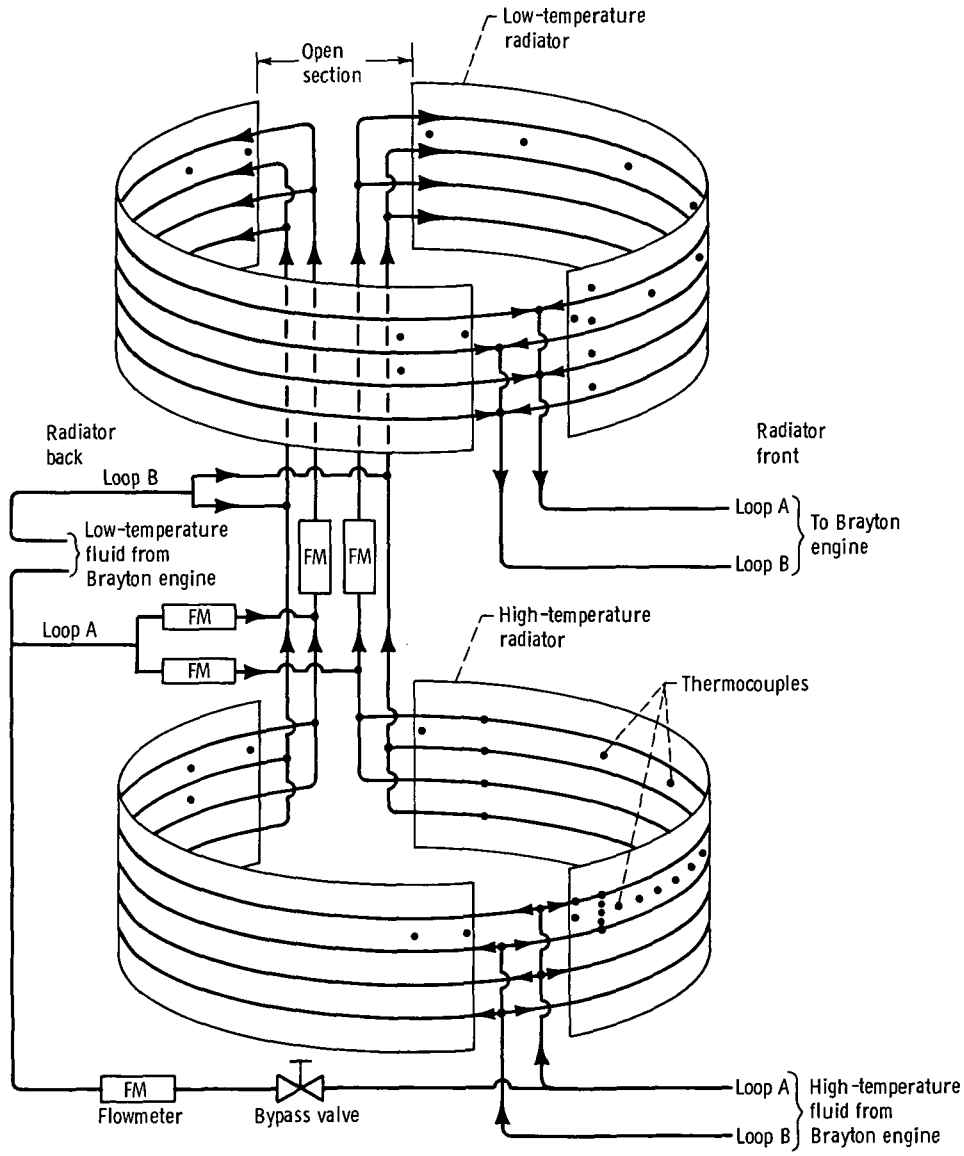

(b) Flow schematic and instrumentation.

Figure 4. - Concluded.

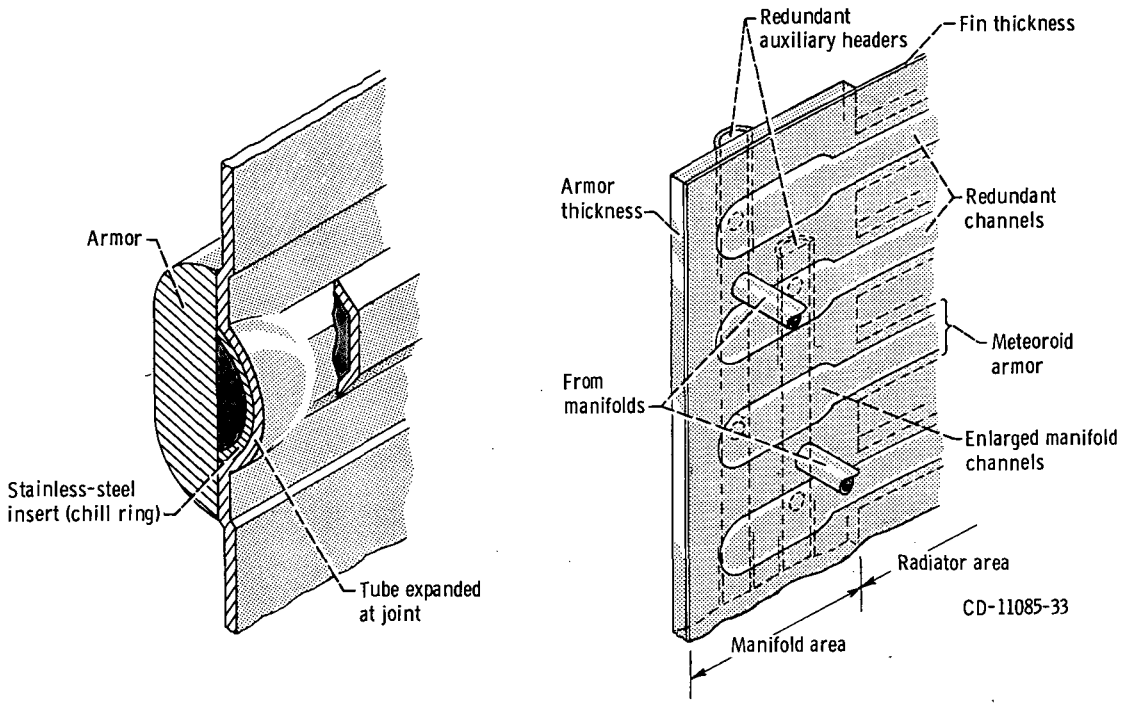

(a) Channel joint.

(b) Radiator assembly (inside view).

Figure 5. - Details of Brayton-cycle radiator-panel channel joint and manifold.

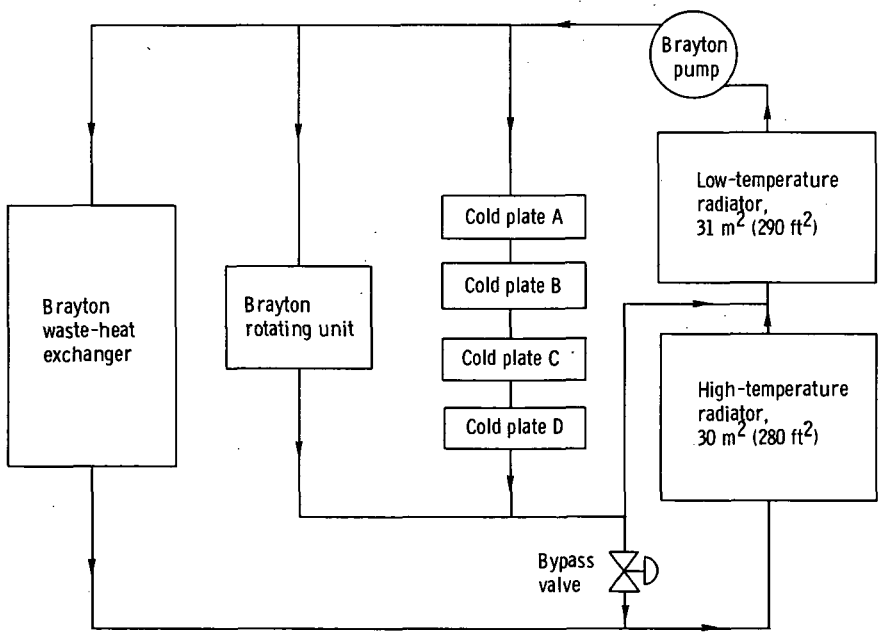

Figure 6. - Actual test schematic of Brayton-cycle coolant loop.

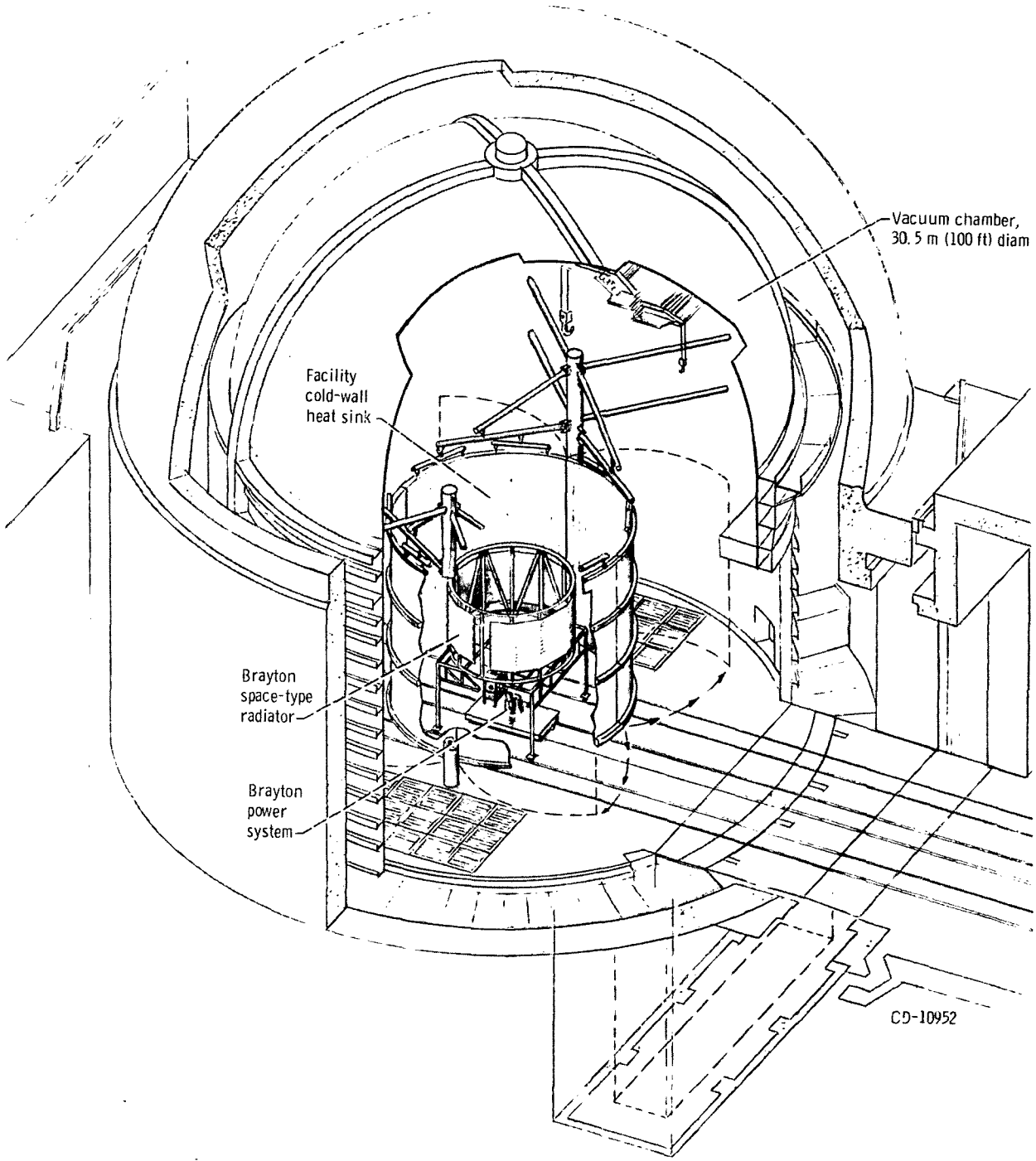

Figure 7. - Illustration of Brayton power system installed for testing in Space Power Facility.

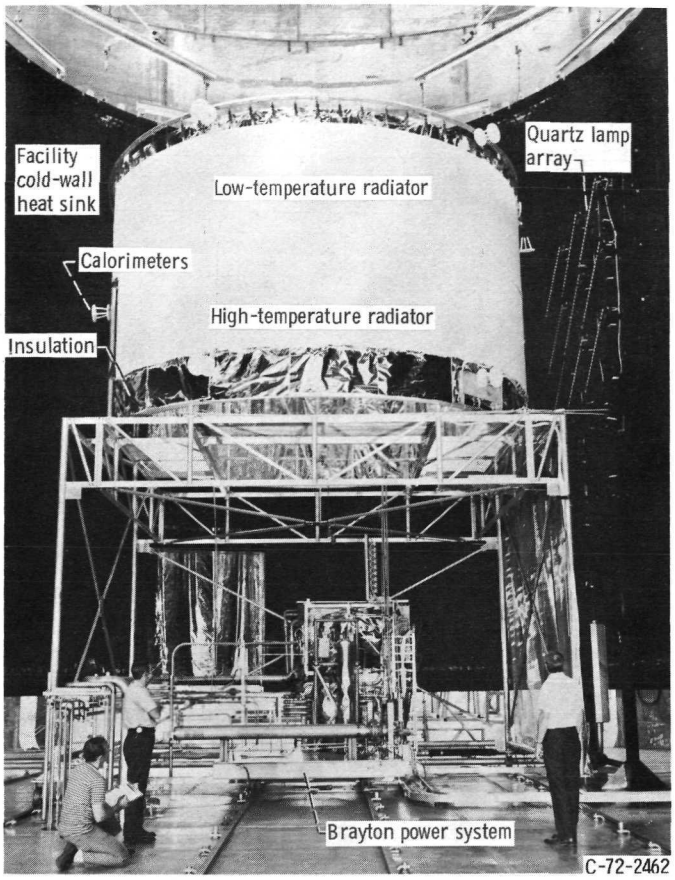

Figure 8. - Brayton power system installed for testing in Space Power Facility.

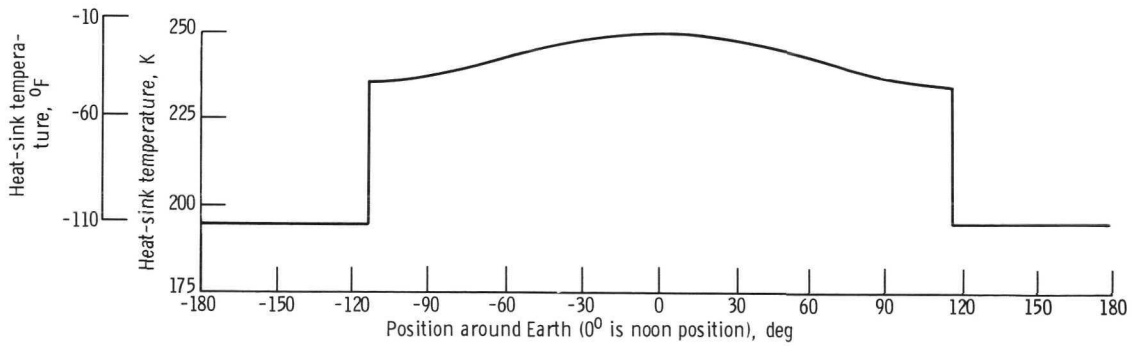

Figure 9. - Sink temperature of radiator "belly" down in low earth orbit. Simulated altitude, ~500 kilometers; emissivity, 0.93; absorptivity, 0.22.

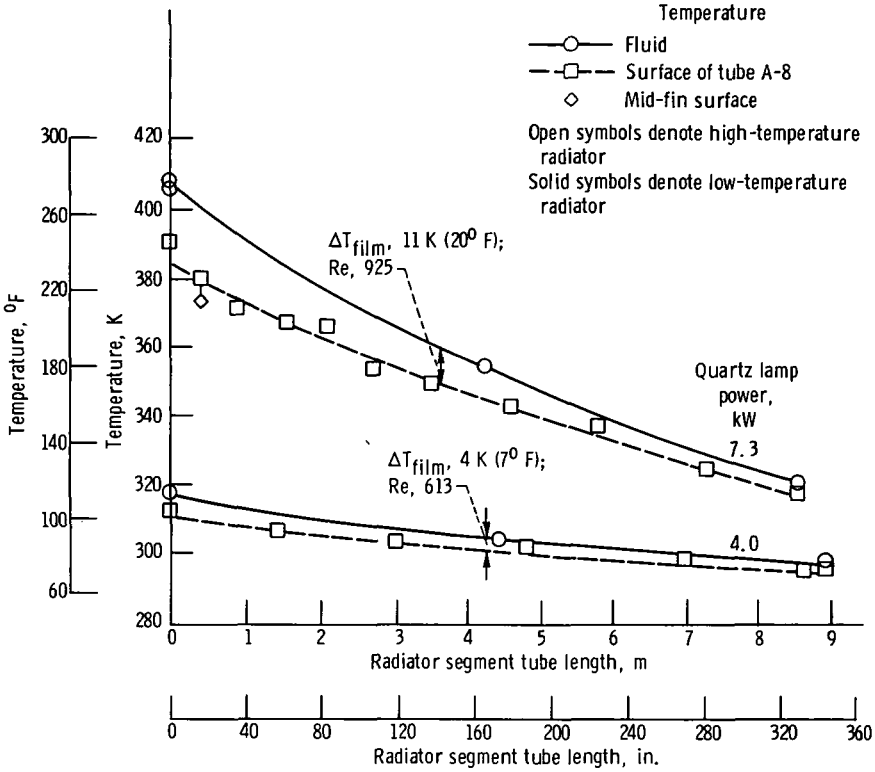

Figure 10. - Fluid and surface temperature profiles for high- and low-temperature radiators at steady-state operation near design point. Heat-sink temperature, 250 K (-10° F).

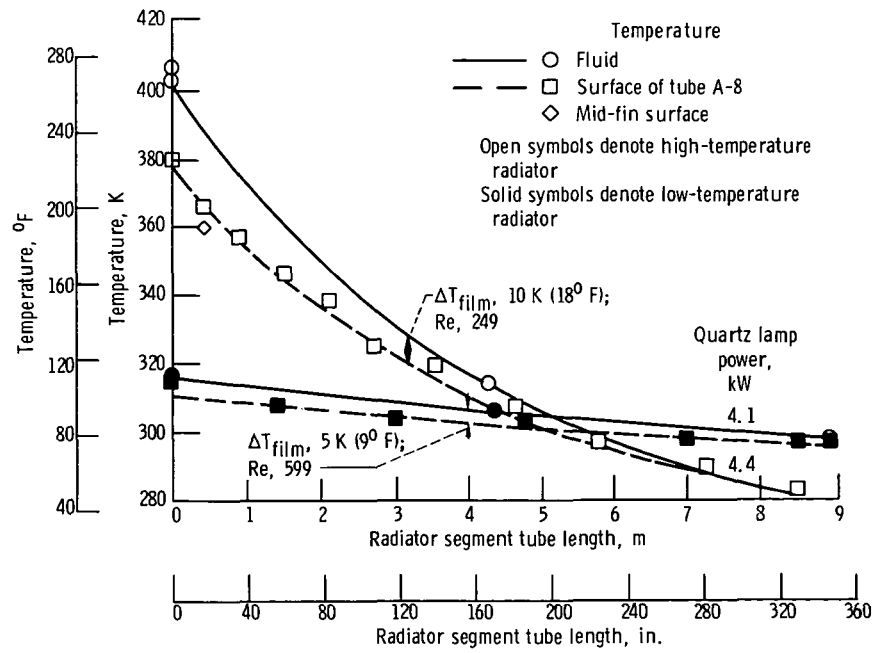

Figure 11. - Fluid and surface temperature profiles for high- and low-temperature radiators at steady-state operation with 35 percent bypass flow. Heat-sink temperature, 250 K (-10° F).

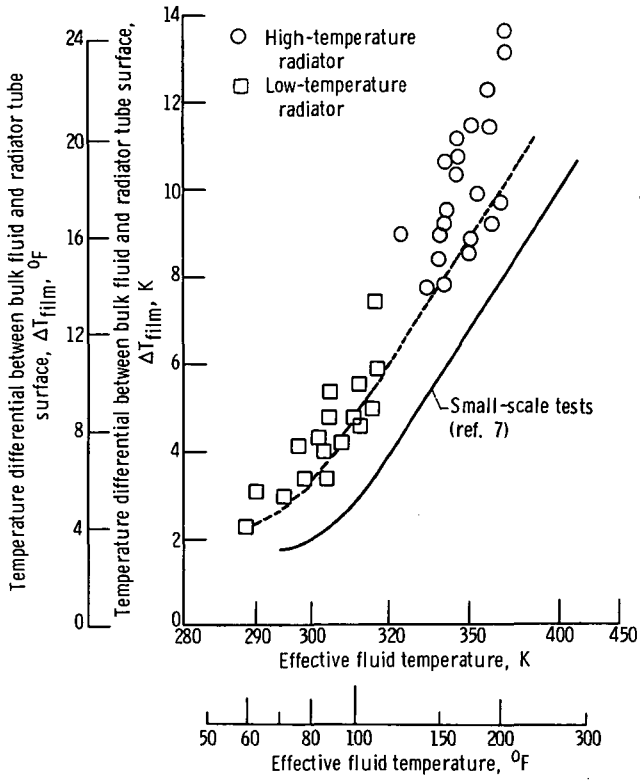

Figure 12. - Temperature differential between bulk fluid and radiator tube surface as function of effective radiator fluid temperature. Heat-sink temperature, 250 K (-10^{o} F); Reynolds number, 300 < Re < 1200.

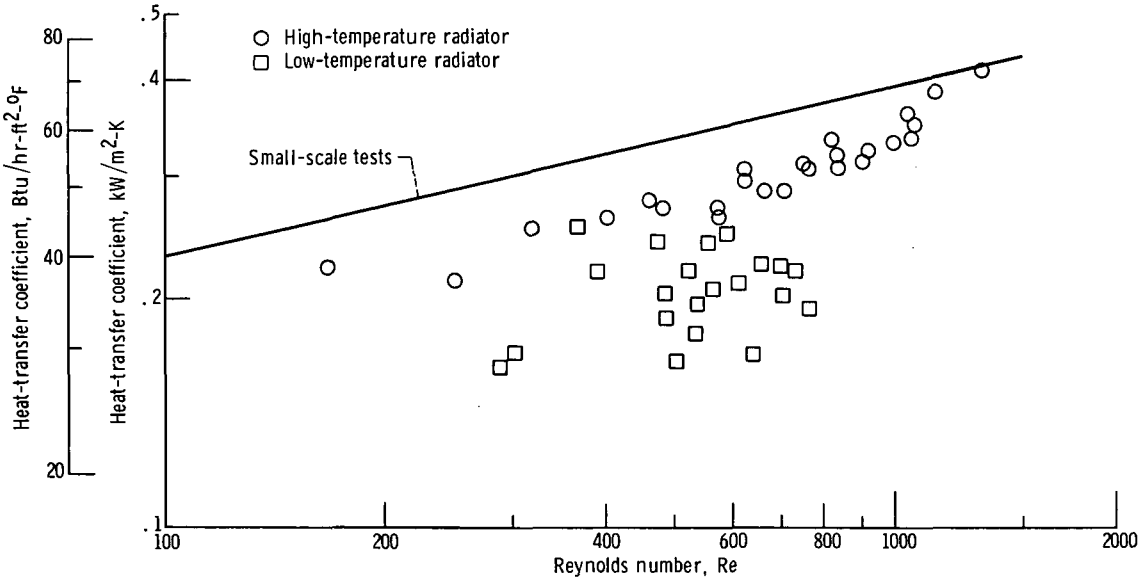

Figure 13. - Variation of steady-state heat-transfer coefficient with Reynolds number.

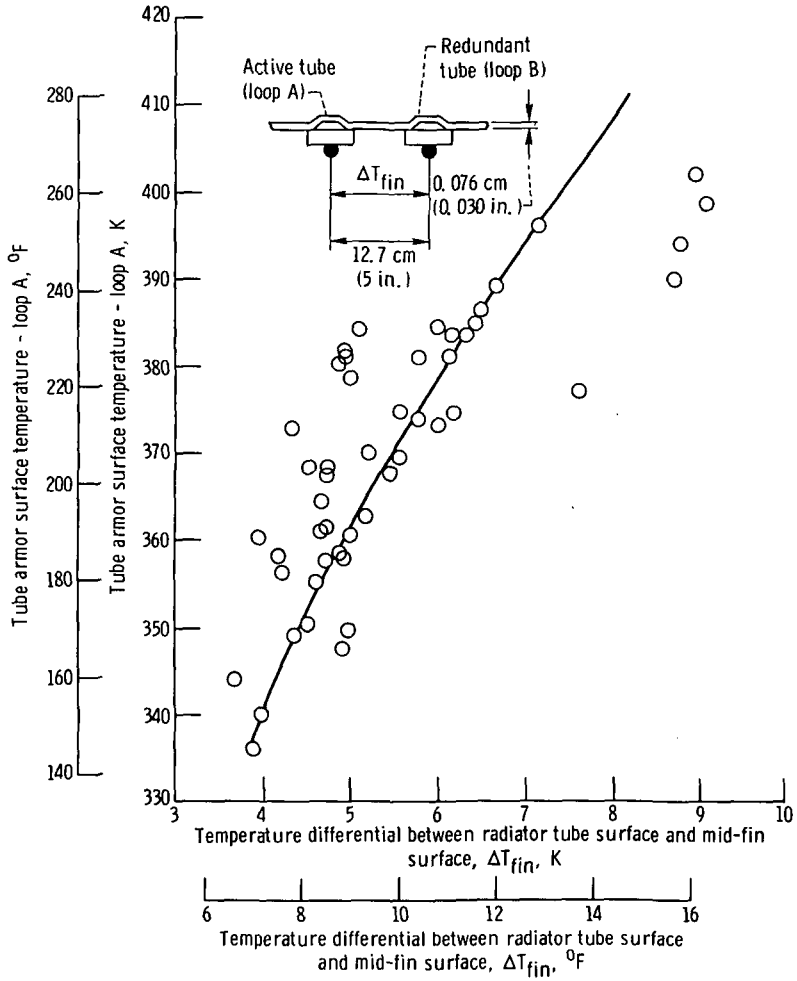

Figure 14. - Mid-fin temperature drop for the high-temperature radiator dissipating to 250 K (-10° F) sink.

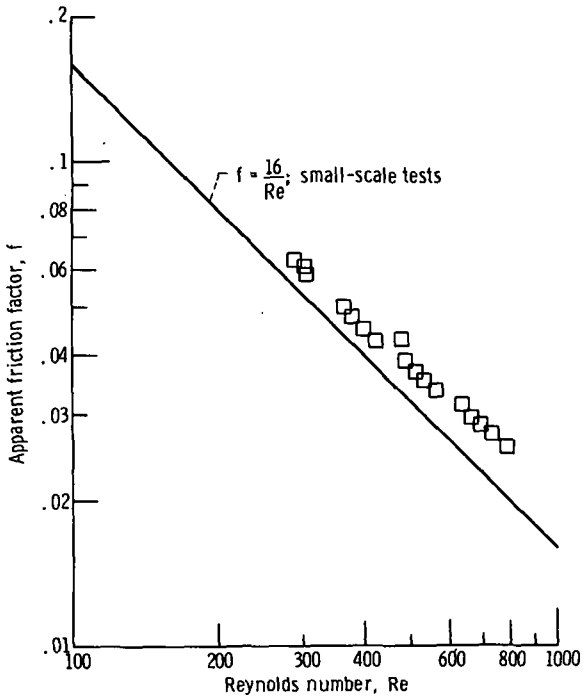

Figure 15. - Laminar-flow friction factor for low-temperature radiator.

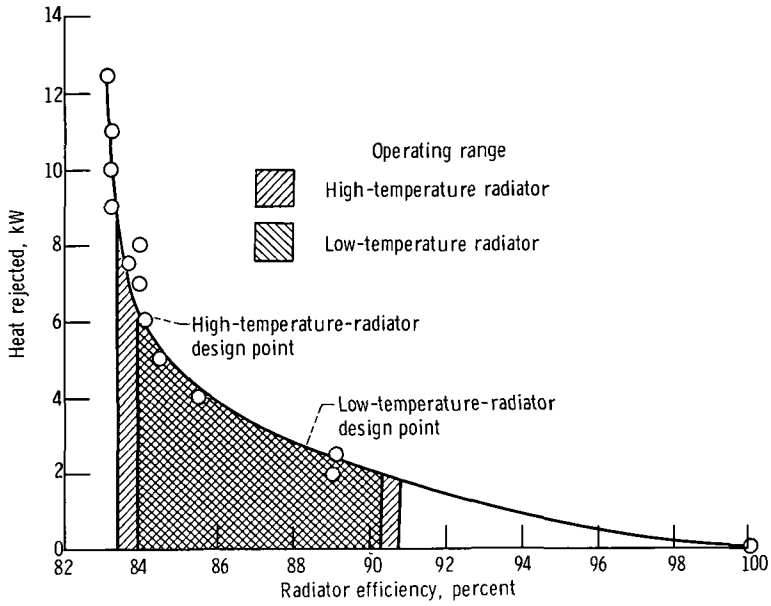

Figure 16. - Efficiency of fixed-area radiator as a function of heat rejected. Heat-sink temperature, 250 K (-10° F).

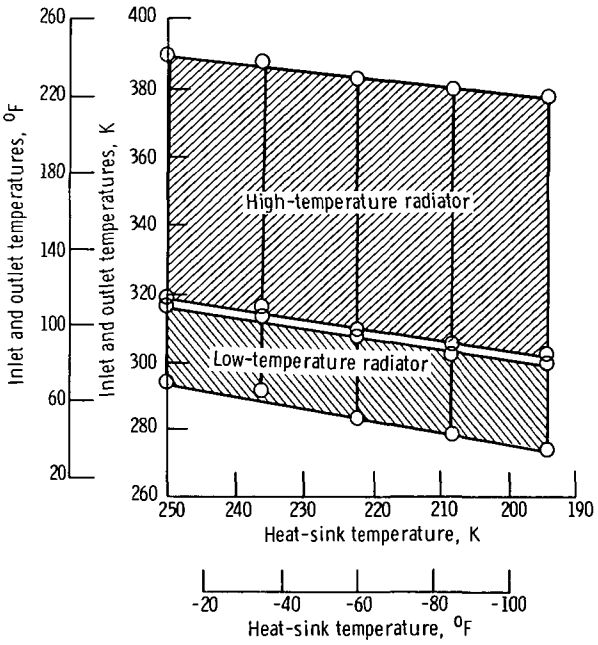

Figure 17. - Range of radiator operating temperatures required to achieve constant total heat rejection at constant flow rates and various heat-sink temperatures. Total heat rejected, 11 kilowatts; flow rate, g/sec(lbm/sec): high-temperature radiator, 43 (0.095); low-temperature radiator, 95 (0.210).

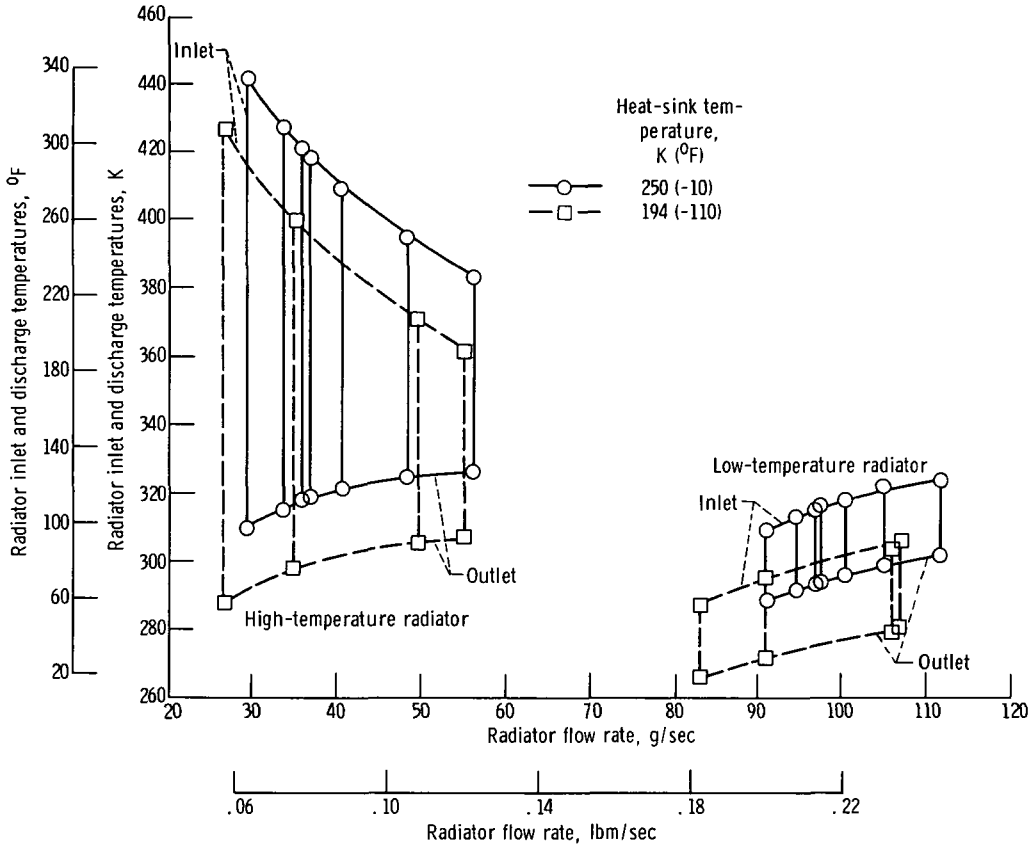

Figure 18. - Range of radiator operating temperatures required to achieve constant total heat rejection at various flow rates. Total heat rejected, 11 kilowatts.

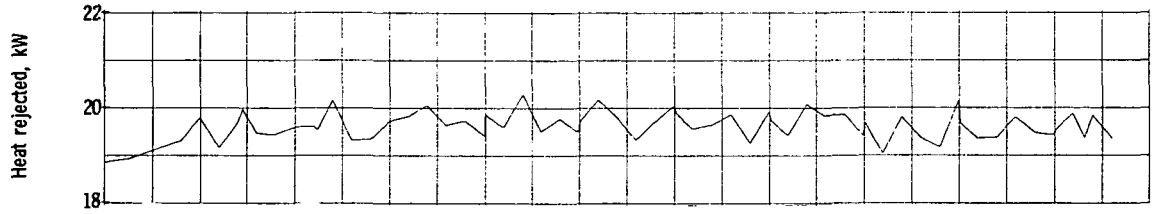

(a) On total radiator heat rejection.

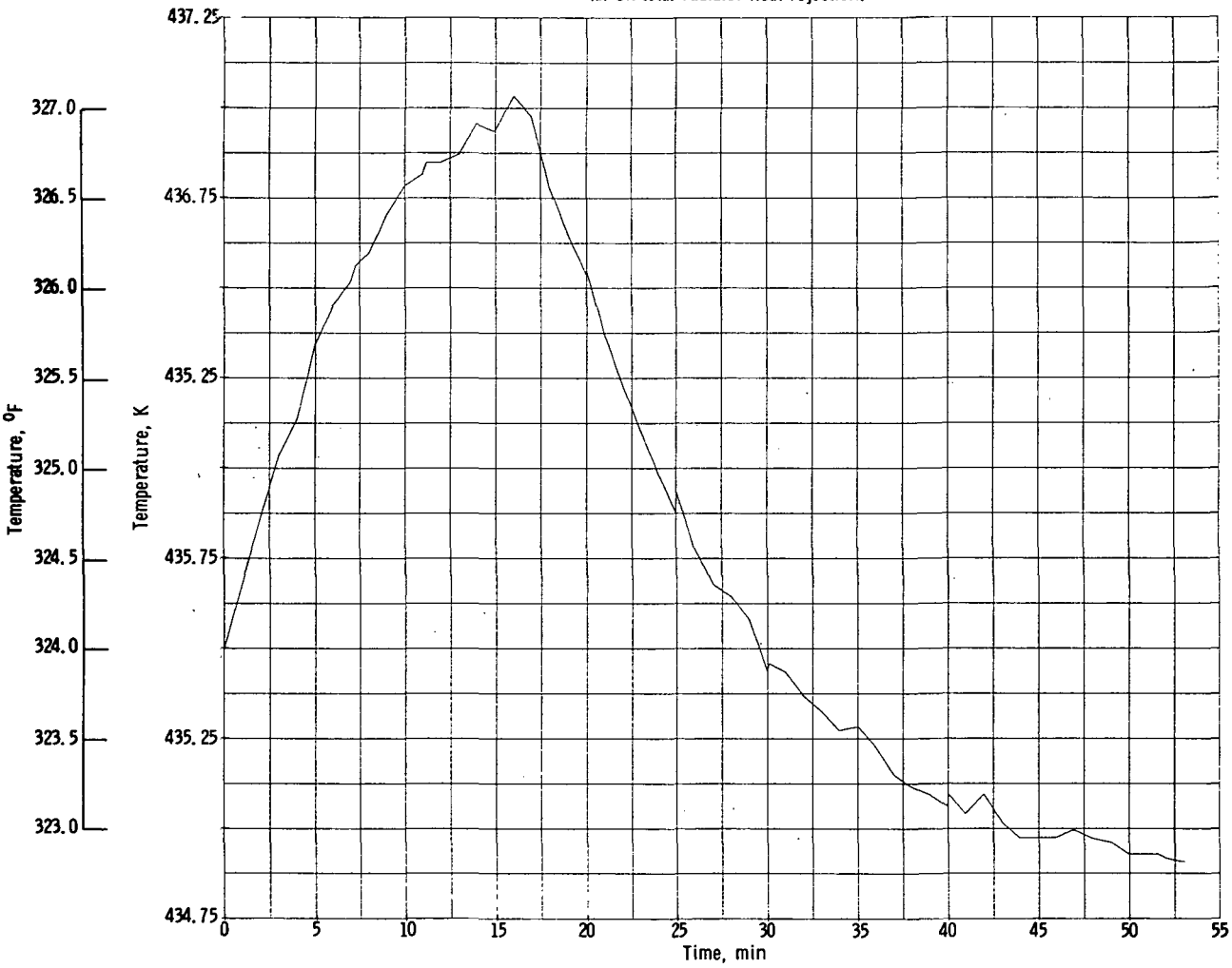

(b) On fluid temperature into high-temperature radiator.

Figure 19. - Effect of 12.5 percent step decrease in fluid flow through high-temperature radiator.

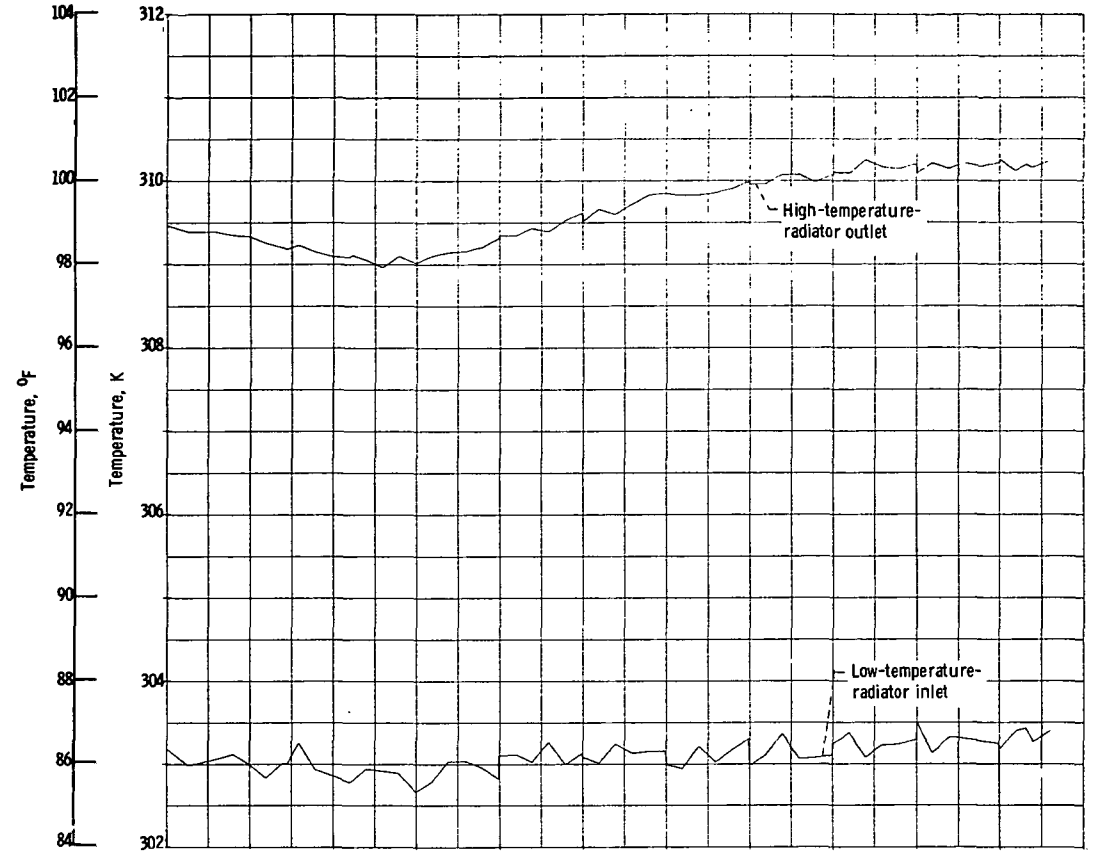

(c) On high-temperature-radiator fluid outlet temperature and on low-temperature-radiator fluid inlet temperature.

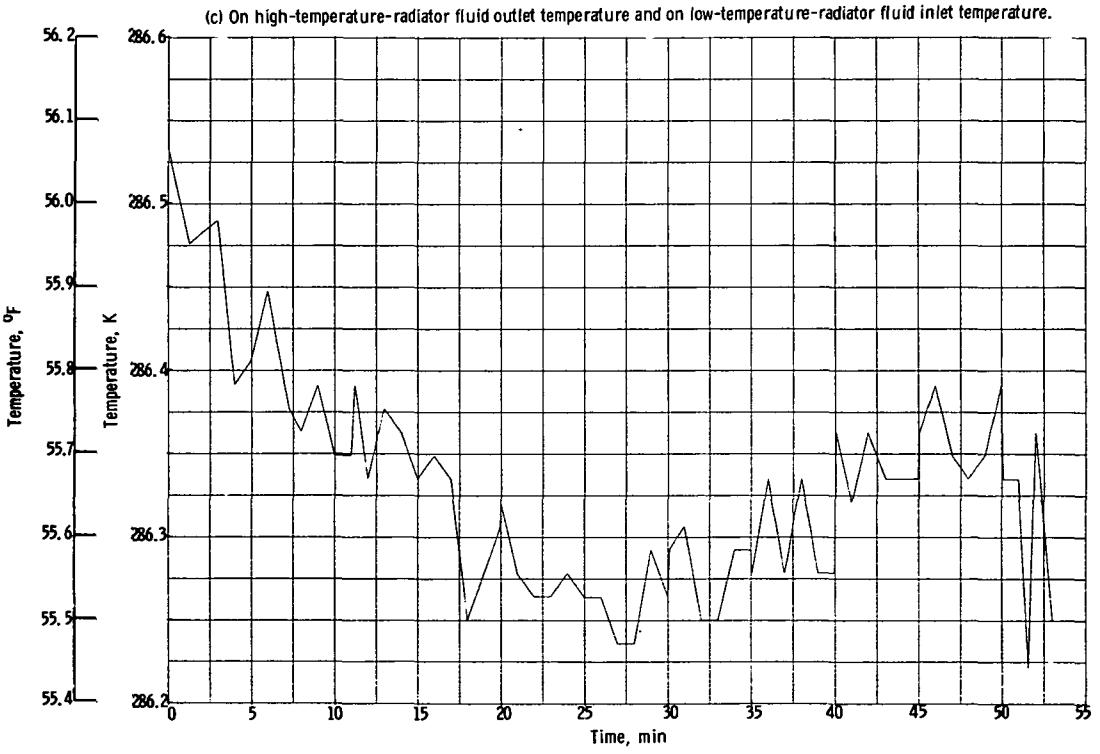

(d) On radiator fluid outlet temperature.

Figure 19. - Concluded.

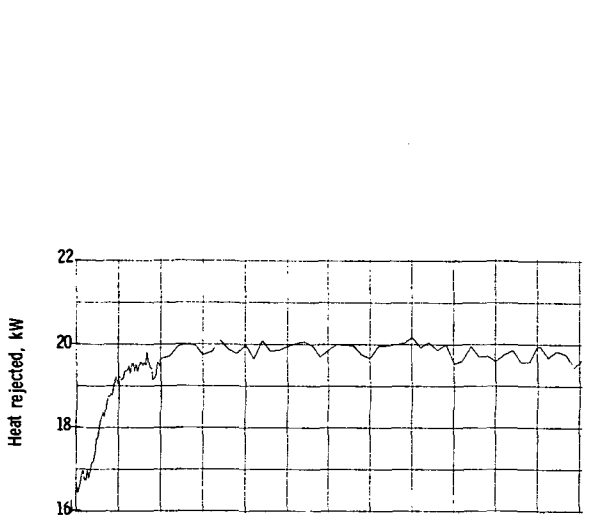

(a) On total radiator heat rejection.

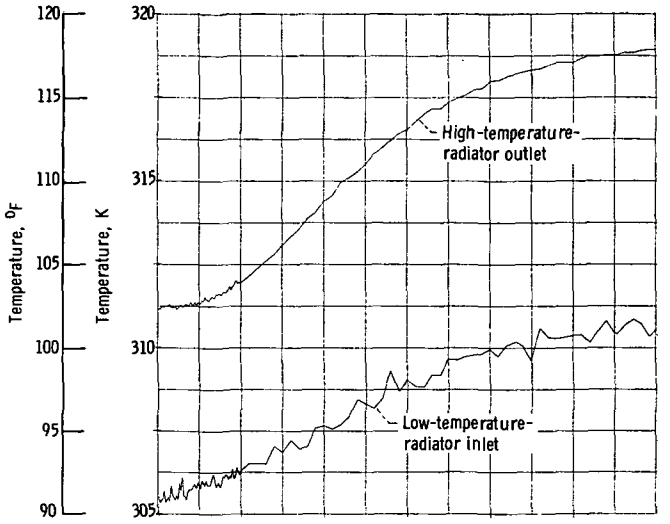

(c) On high-temperature-radiator fluid outlet temperature and low-temperature-radiator fluid inlet temperature.

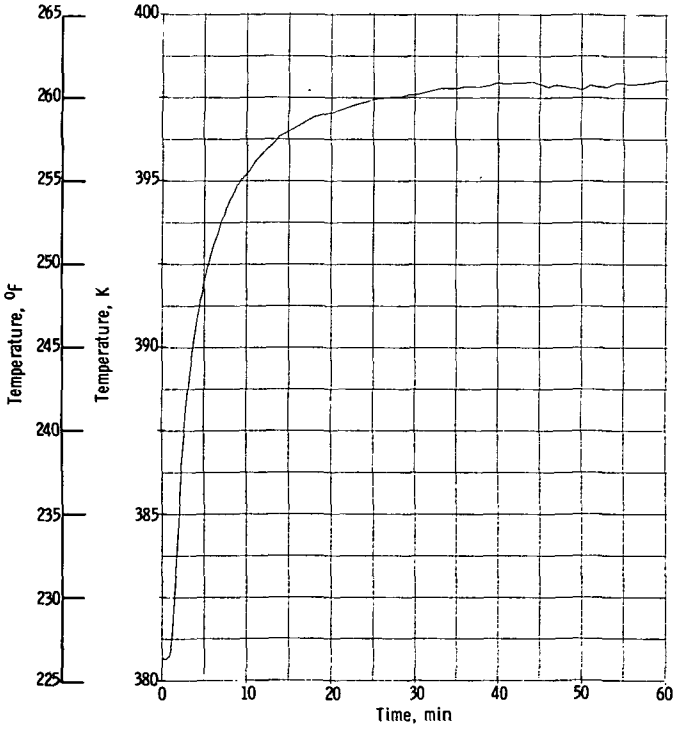

(b) On high-temperature-radiator fluid inlet temperature.

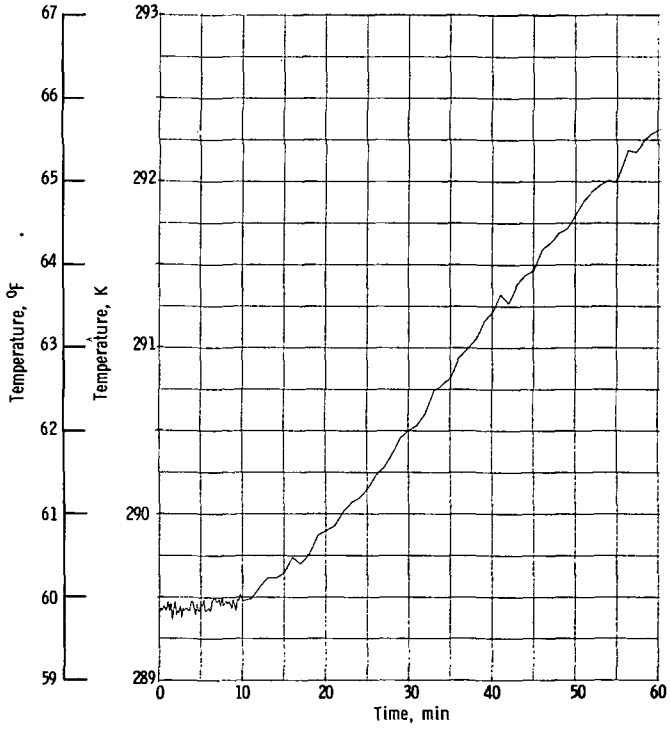

(d) On radiator fluid outlet temperature.

Figure 20. - Effect of 22 percent step increase in Brayton engine compressor discharge pressure.

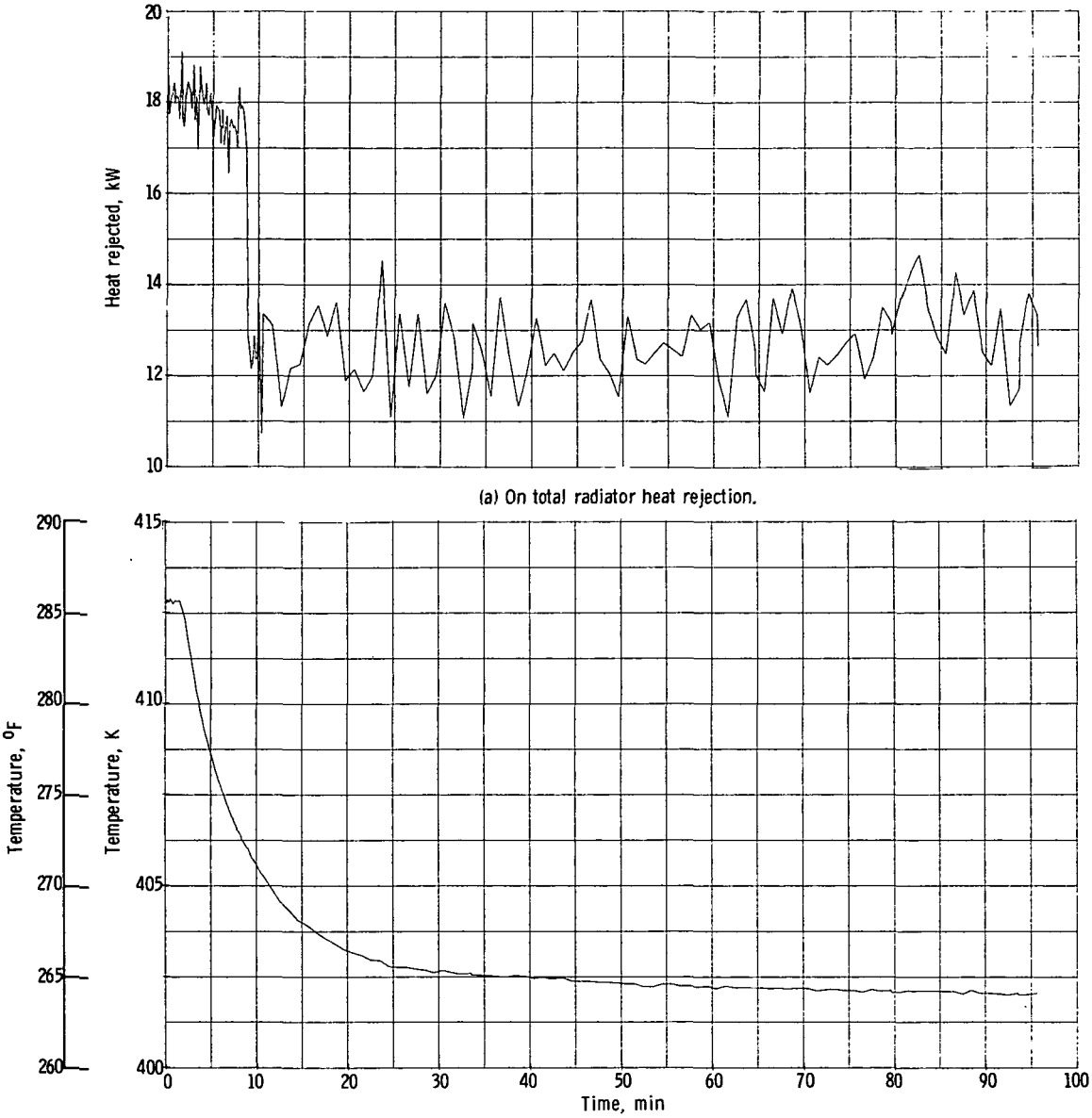

(a) On total radiator heat rejection.

(b) On high-temperature-radiator fluid inlet temperature.

Figure 21. - Effect of 10 percent step decrease in Brayton engine compressor discharge pressure.

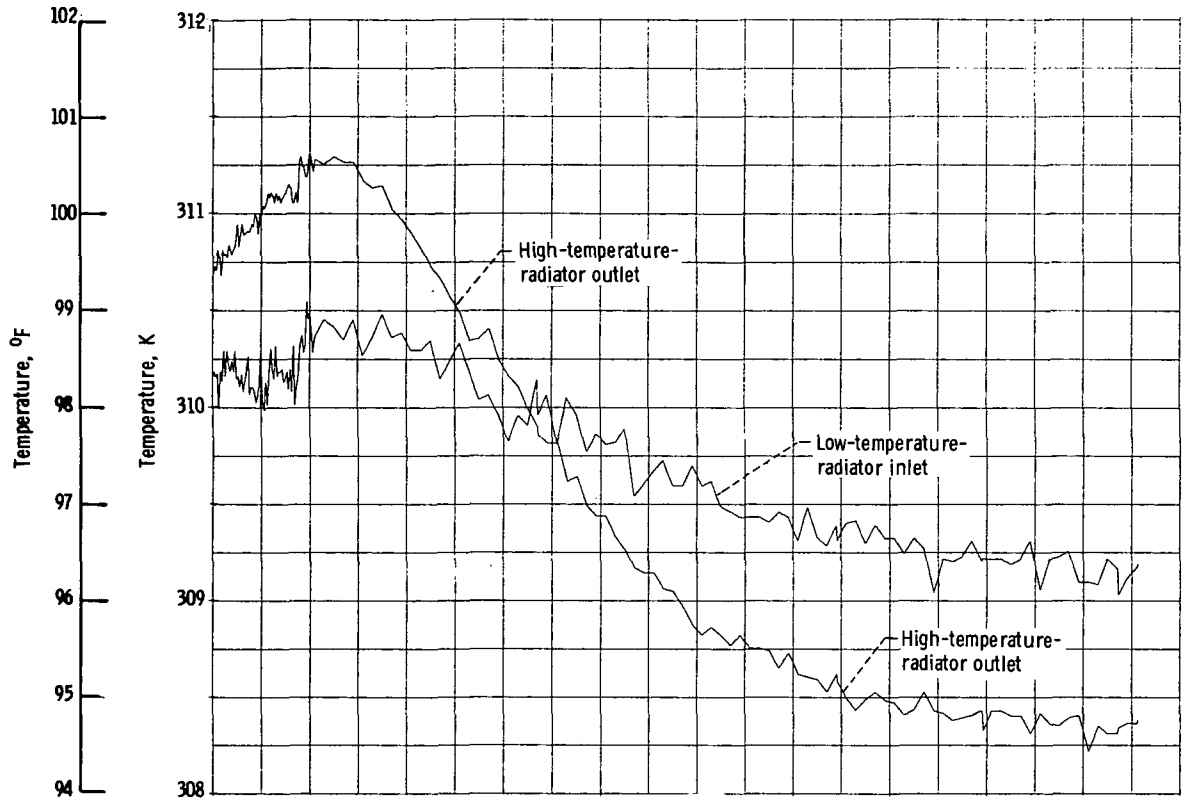

(c) On high-temperature-radiator fluid outlet temperature and on low-temperature-radiator fluid inlet temperature.

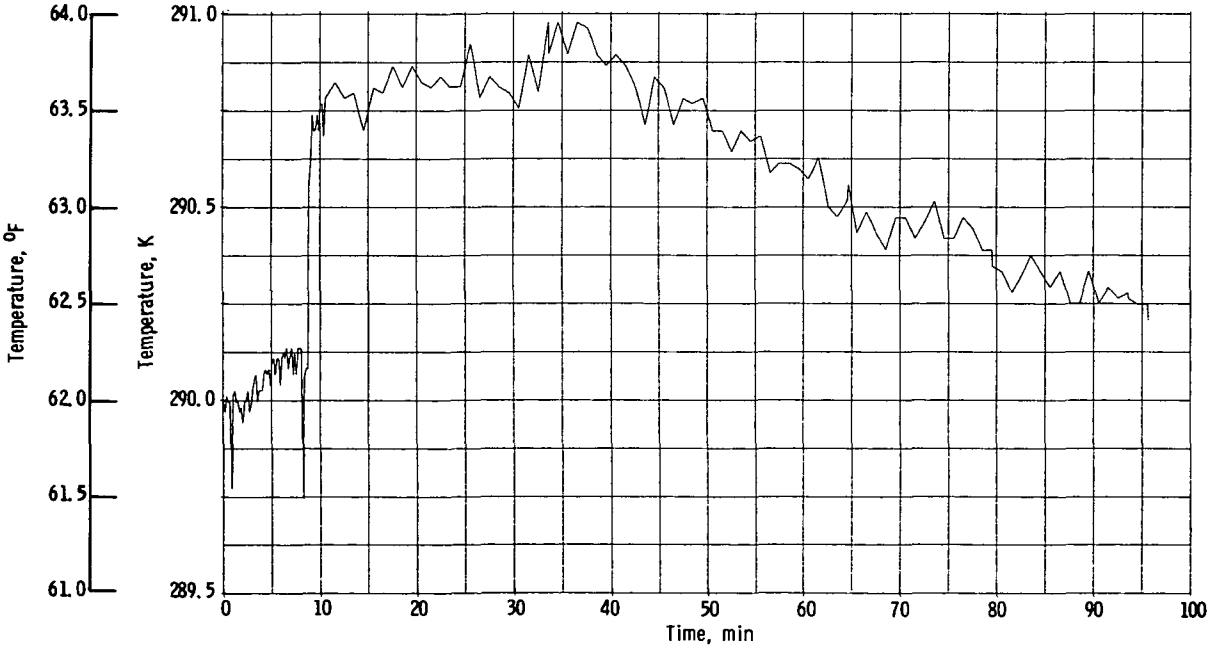

(d) On radiator fluid outlet temperature.

Figure 21. - Concluded.

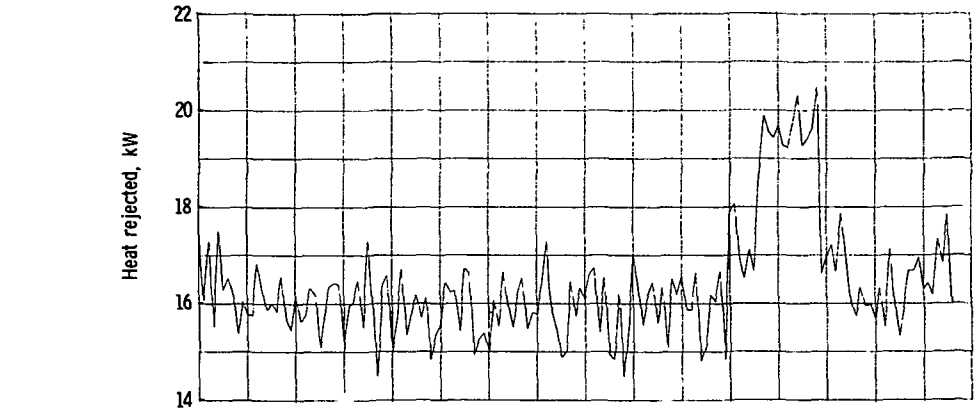

(a) On total radiator heat rejection.

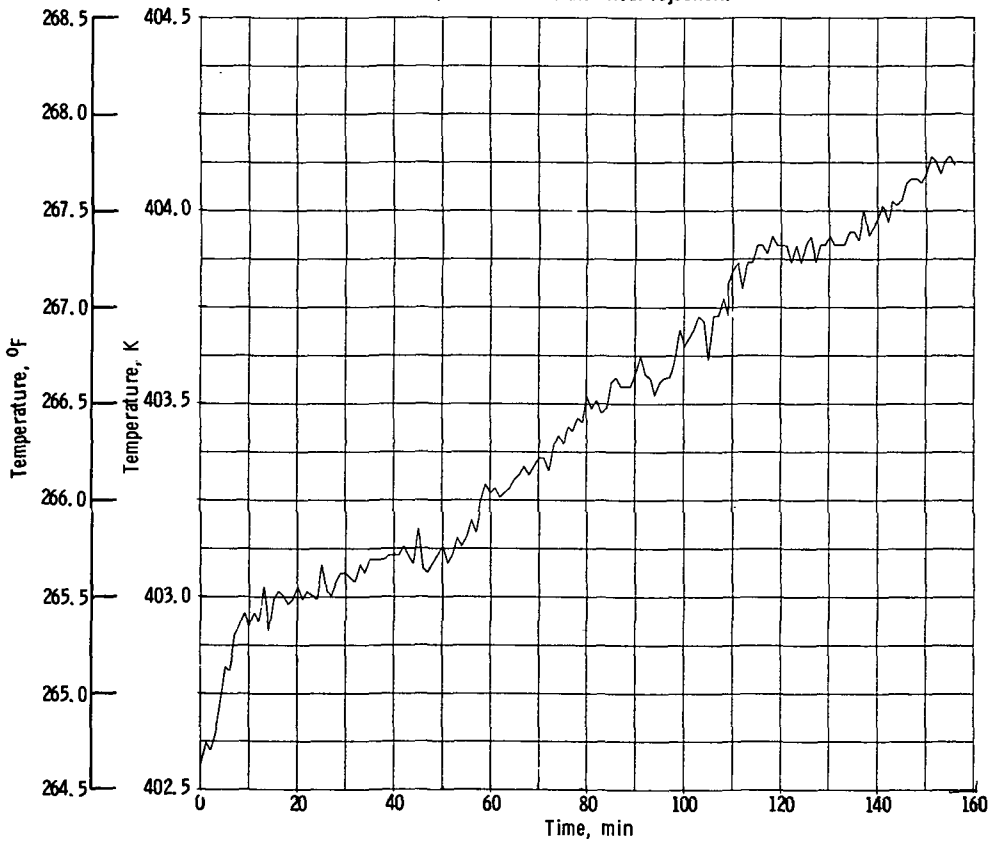

(b) On high-temperature-radiator fluid inlet temperature.

Figure 22. - Effect of increasing Brayton engine turbine inlet temperature from 1030 K to 1090 K (at a rate of 3 K/5 min).

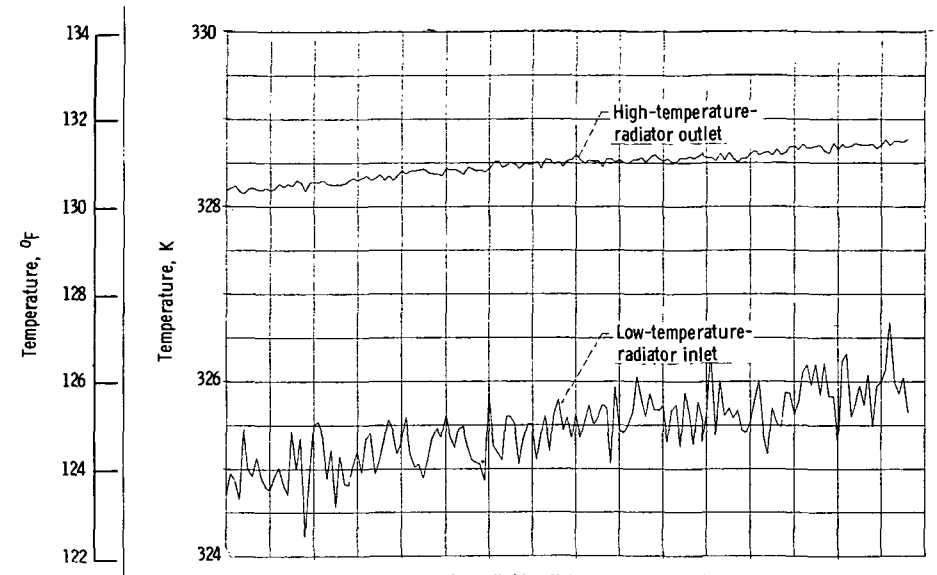

(c) On high-temperature-radiator fluid outlet temperature and on low-temperature-radiator fluid inlet temperature.

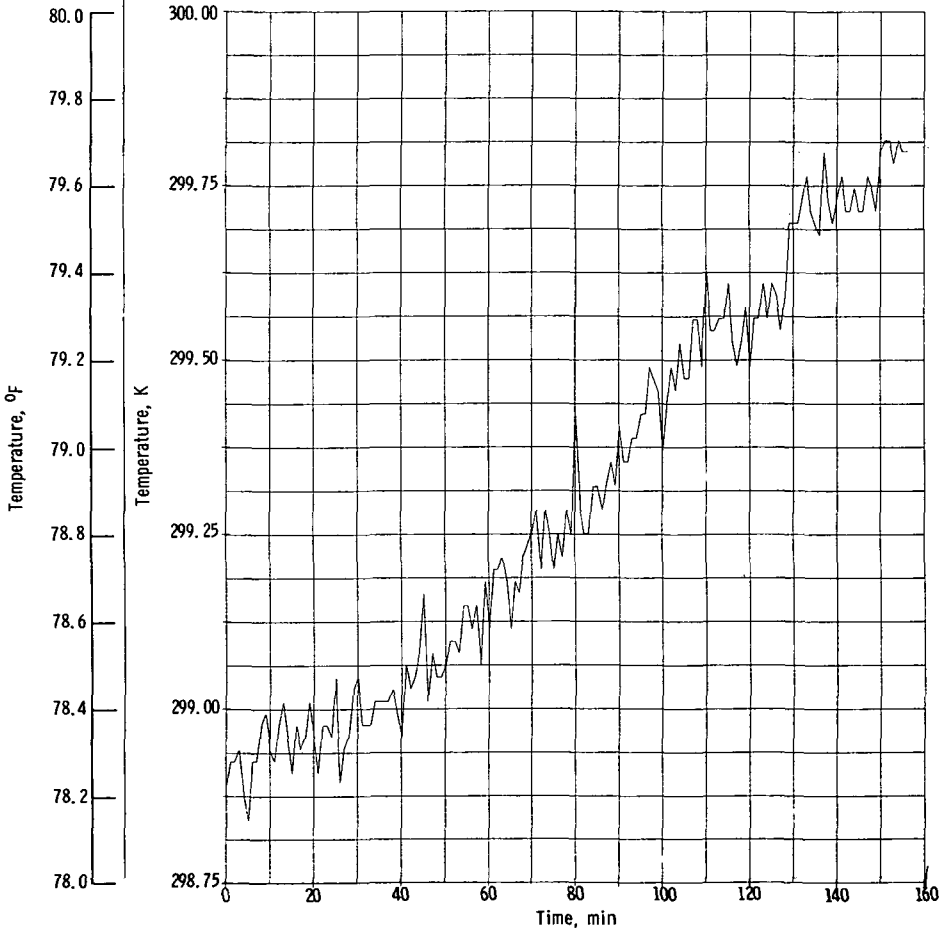

(d) On radiator fluid outlet temperature.

Figure 22. - Concluded.

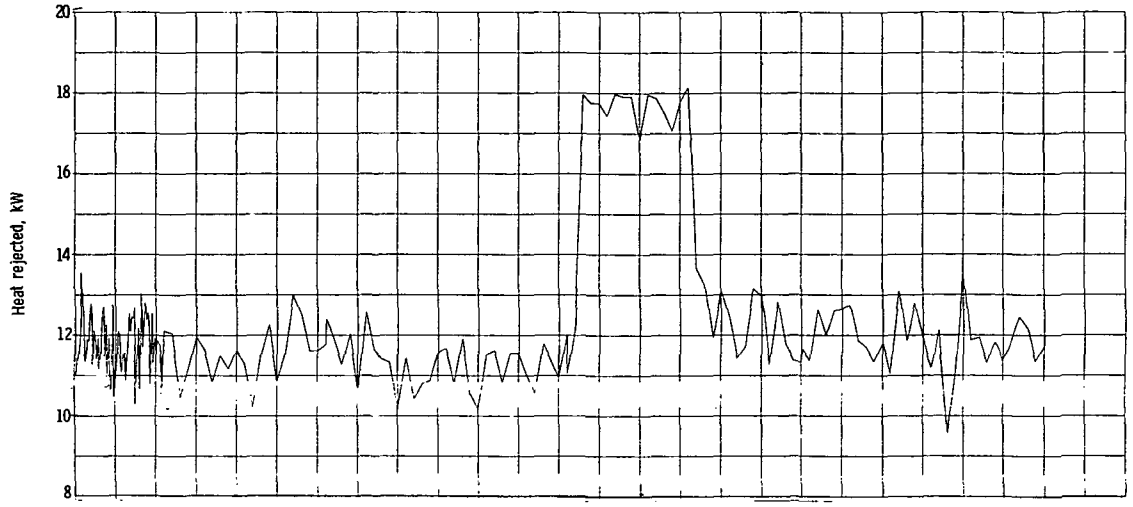

(a) On total radiator heat rejected.

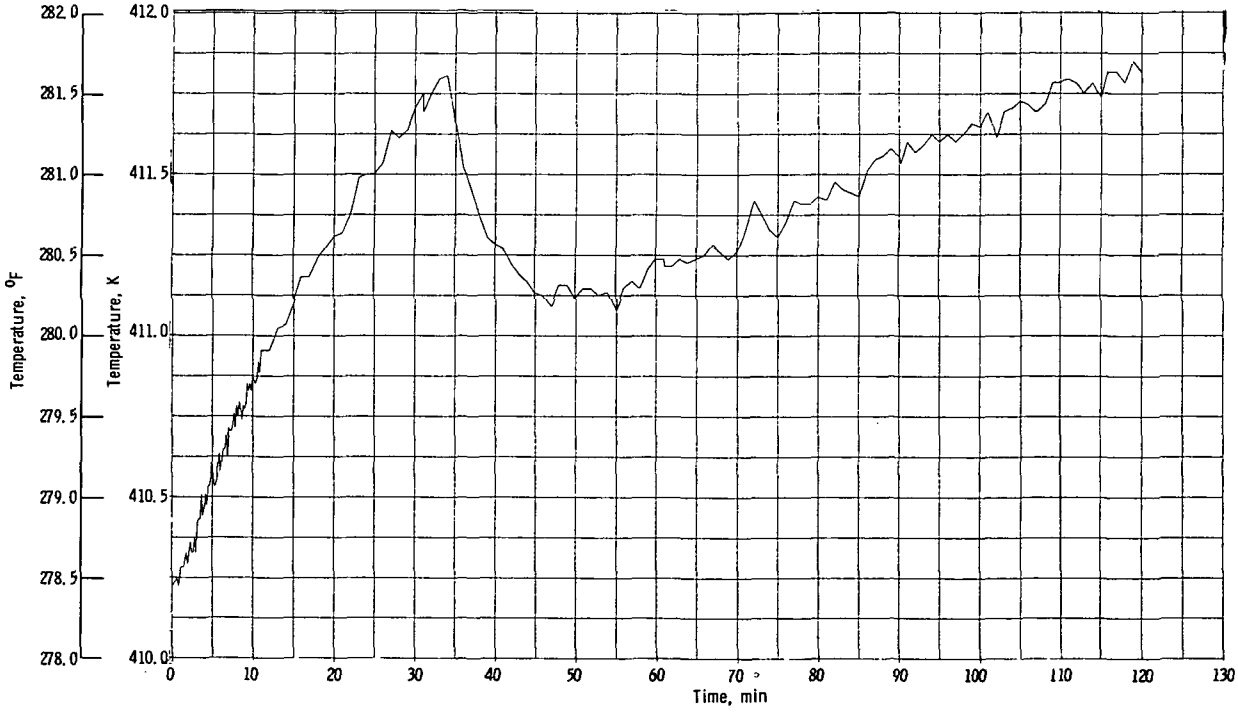

(b) On high-temperature-radiator fluid inlet temperature.

Figure 23. - Effect of 11-kelvin step increase in Brayton engine turbine inlet temperature.

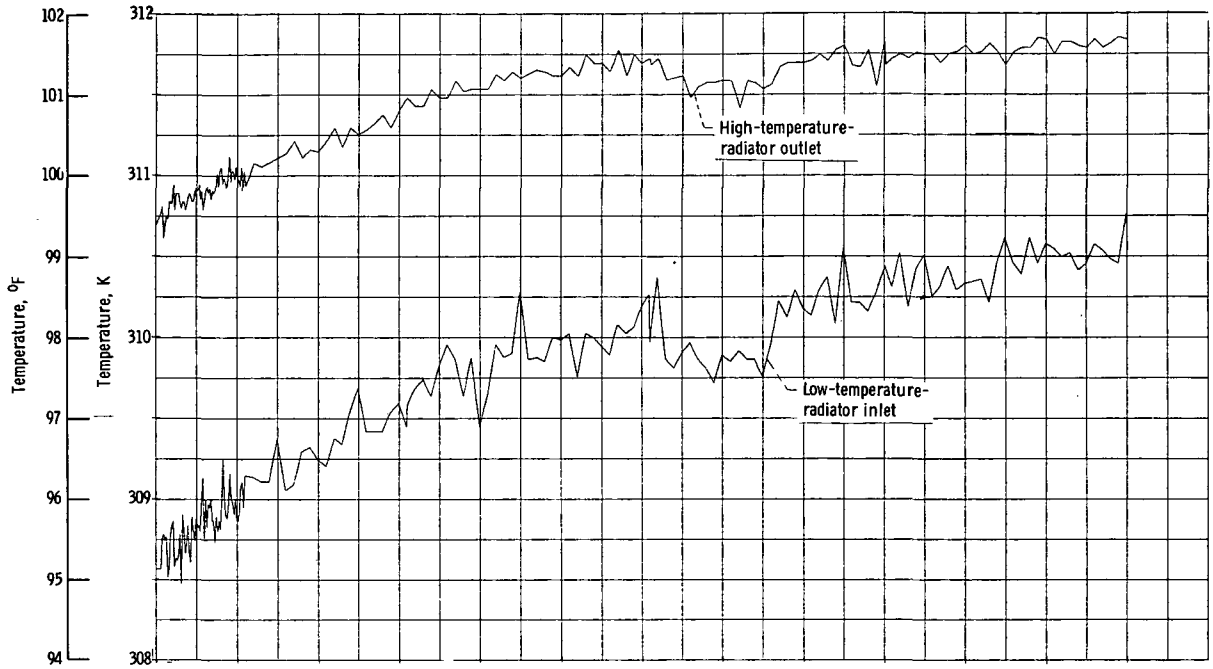

(c) On high-temperature-radiator fluid outlet temperature and on low-temperature-radiator fluid inlet temperature.

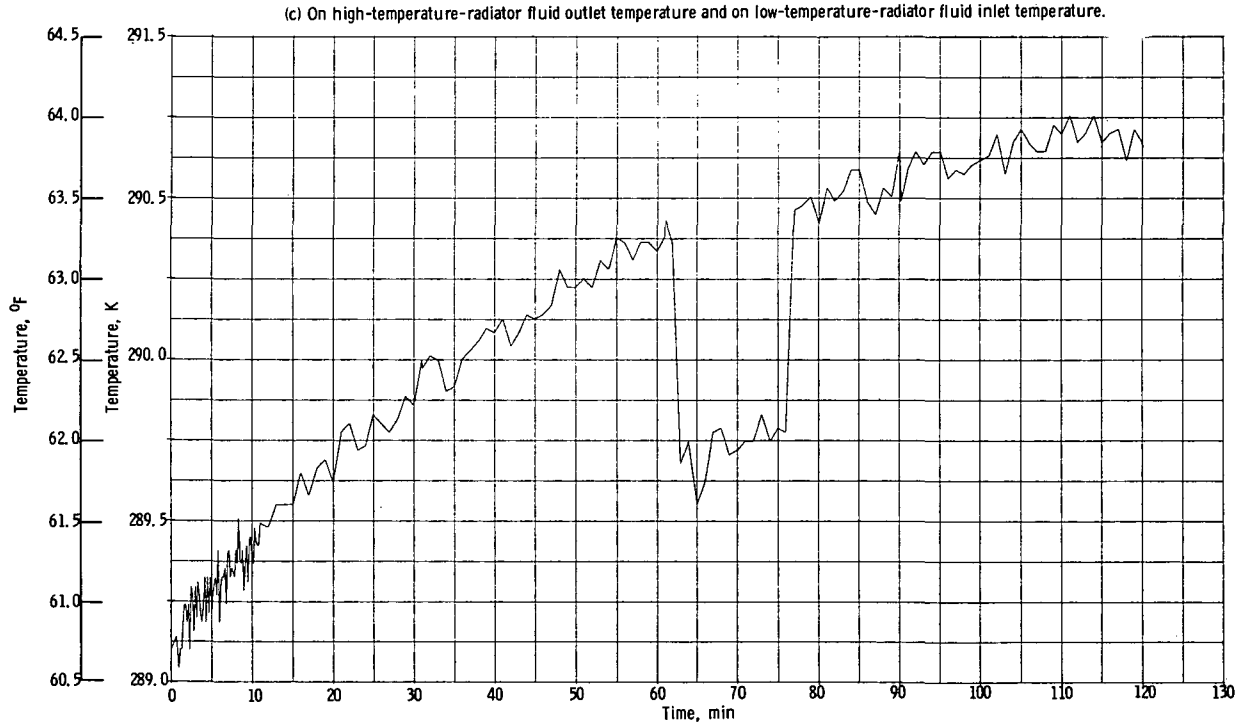

(d) On radiator fluid outlet temperature.

Figure 23. - Concluded.

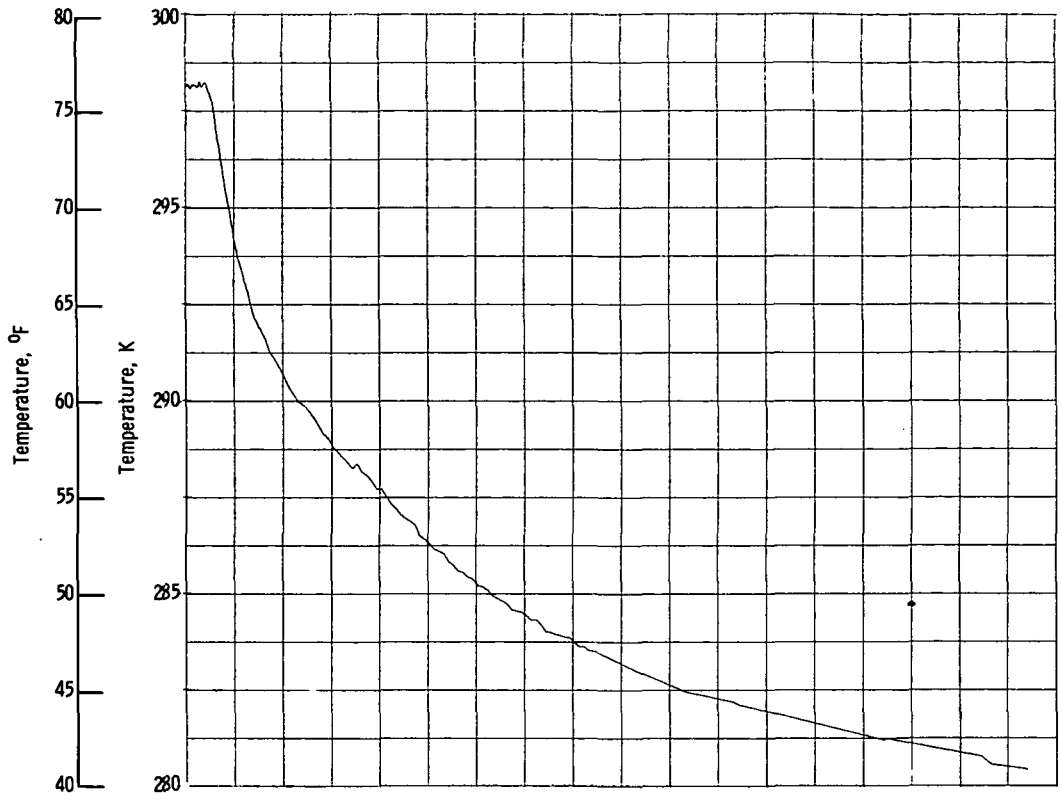

(a) On high-temperature-radiator fluid inlet temperature.

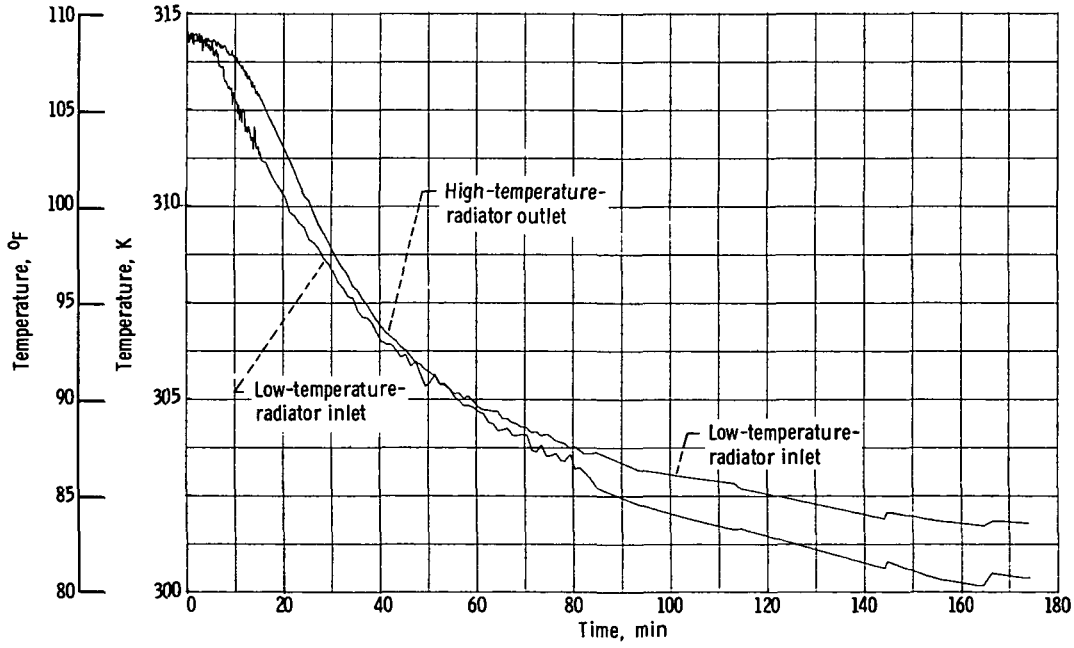

(b) On fluid from high-temperature radiator and on fluid into low-temperature radiator.

Figure 24. - Effect of sun-shade transient. Sun temperature, 256 K; shade temperature, 195 K.

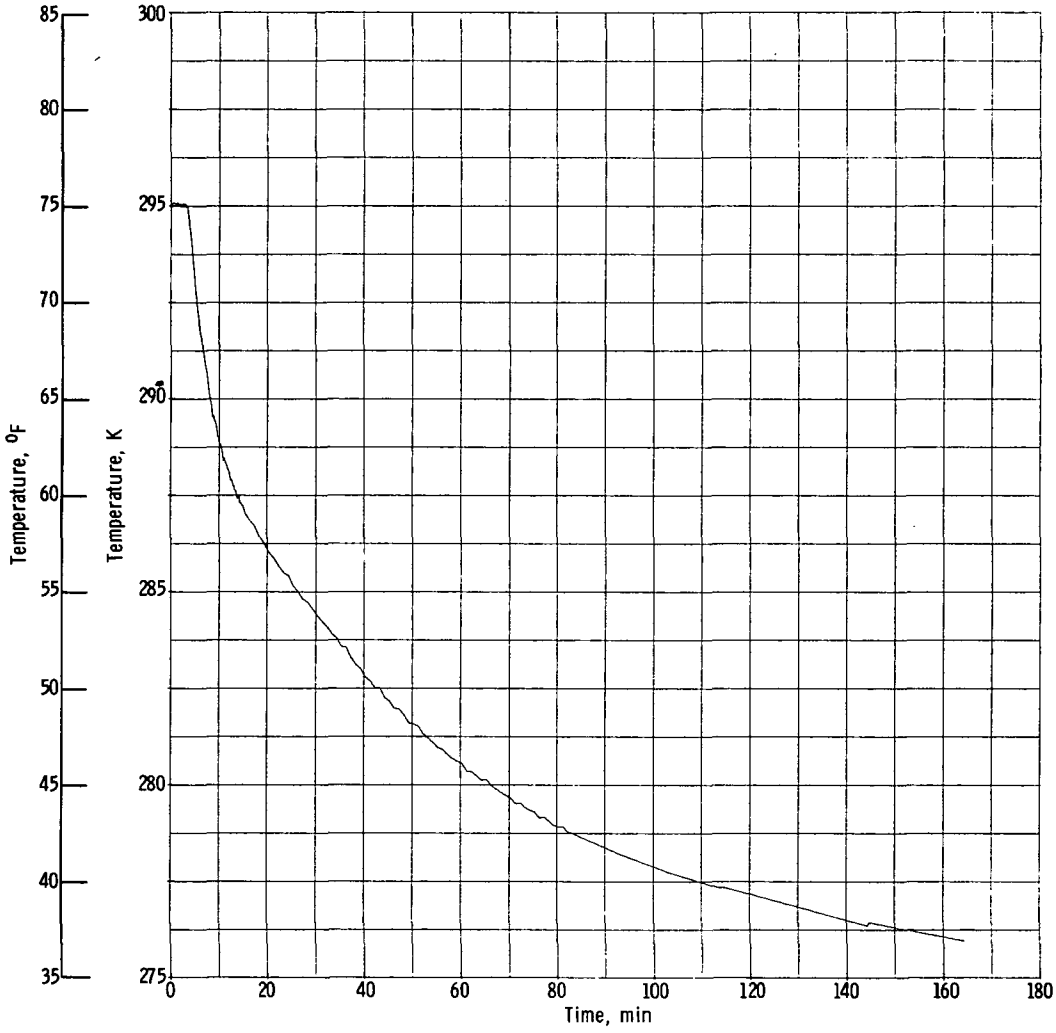

(c) On radiator fluid outlet temperature.

Figure 24. - Concluded.

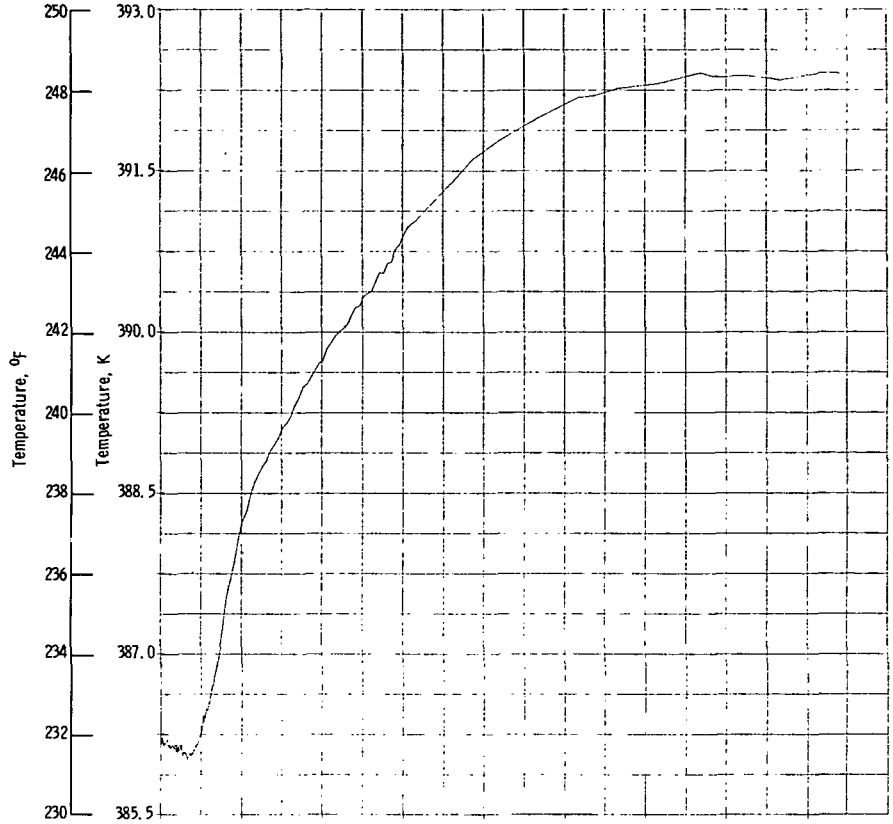

(a) On high-temperature-radiator fluid inlet temperature.

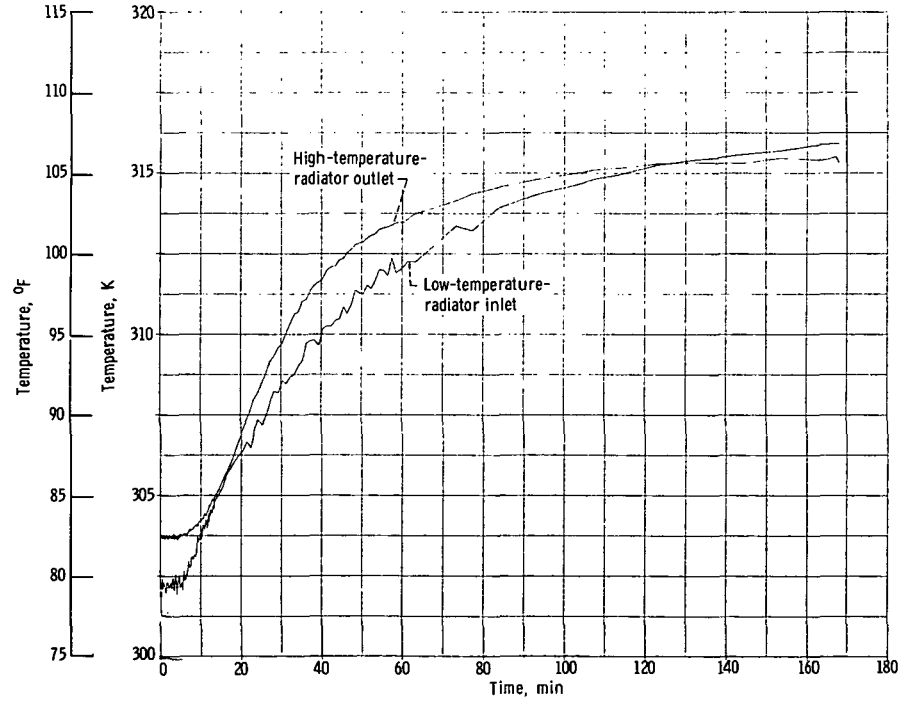

(b) On fluid from high-temperature radiator and on fluid into low-temperature radiator.

Figure 25. - Effect of shade-sun transient. Shade temperature, 195 K; sun temperature, 256 K.

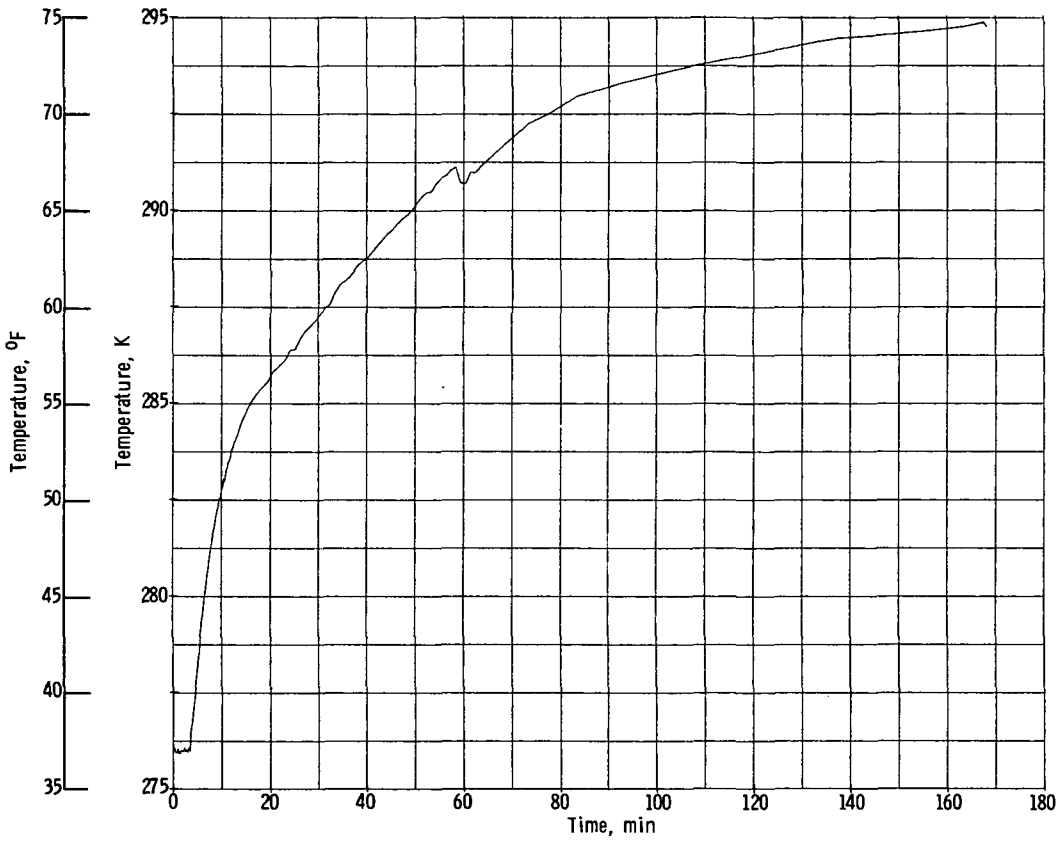

(c) On radiator fluid outlet temperature.

Figure 25. - Concluded.

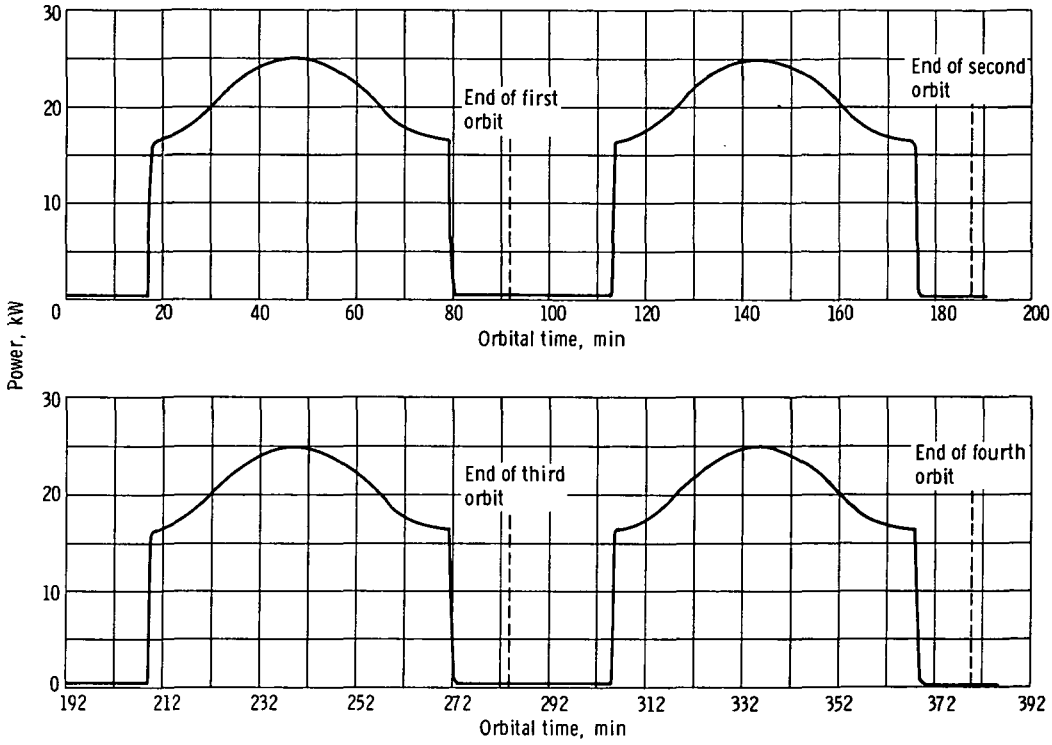

Figure 26. - Power to quartz lamp display as function of orbital time.

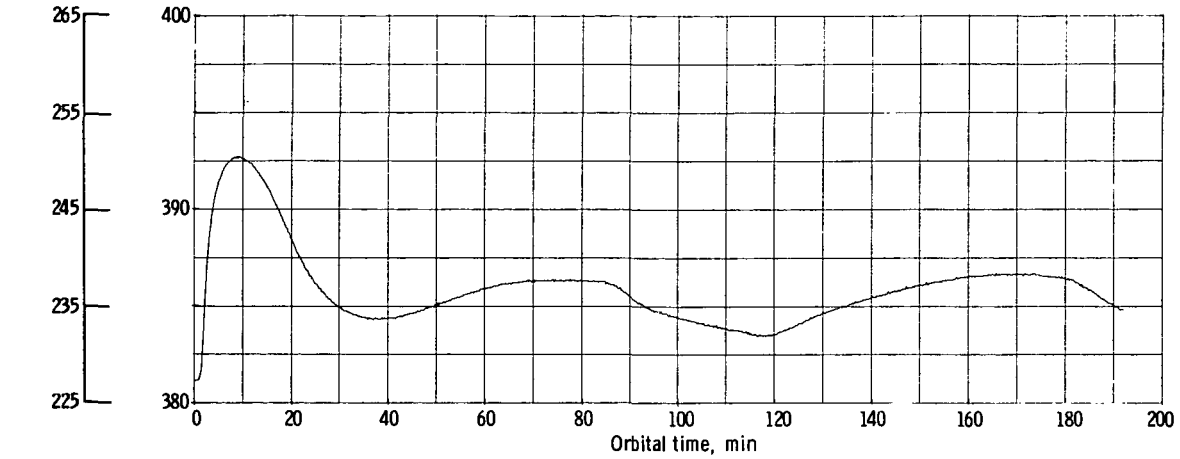

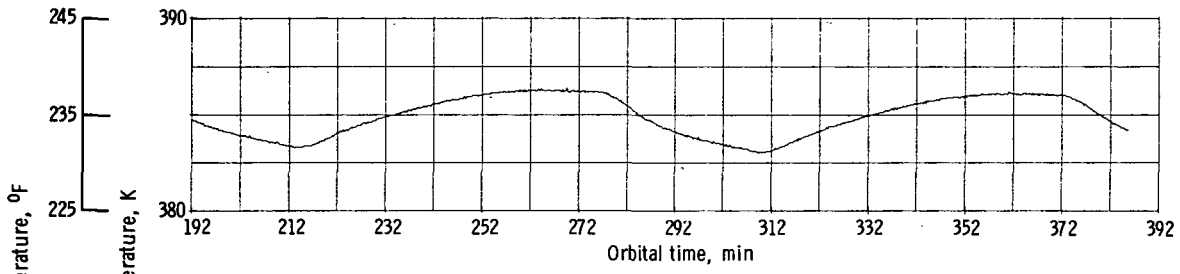

(a) On high-temperature-radiator fluid inlet temperature.

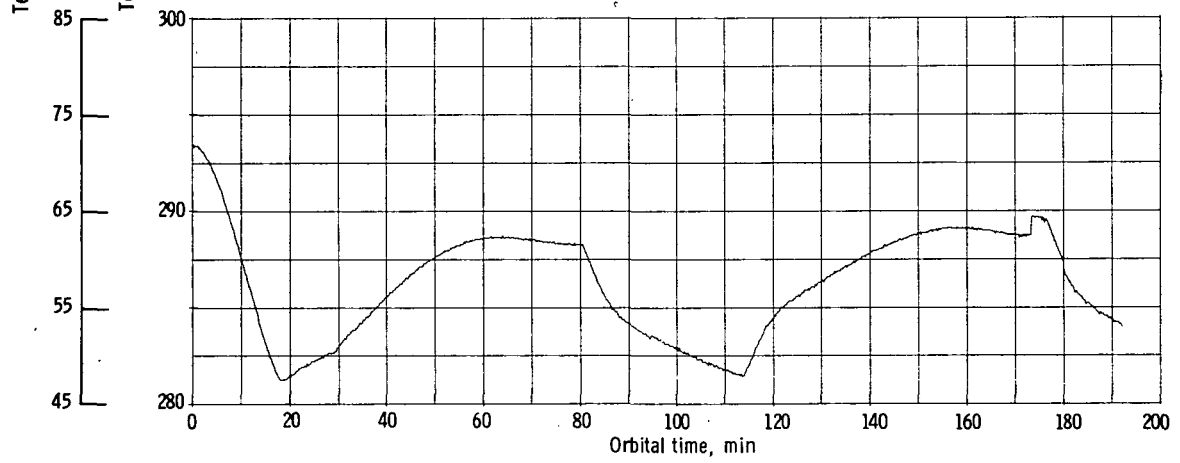

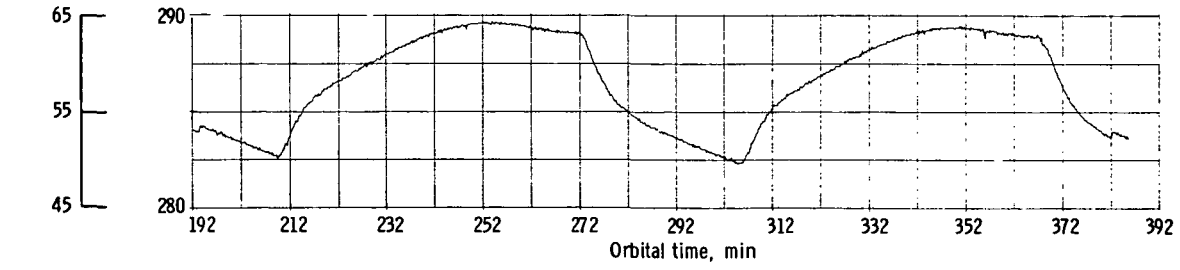

(b) On radiator outlet temperature.

Figure 27. - Effect of engine operation at constant gas inventory and constant turbine inlet temperature on high-temperature-radiator fluid inlet temperature and on radiator outlet temperature as functions of orbital time.

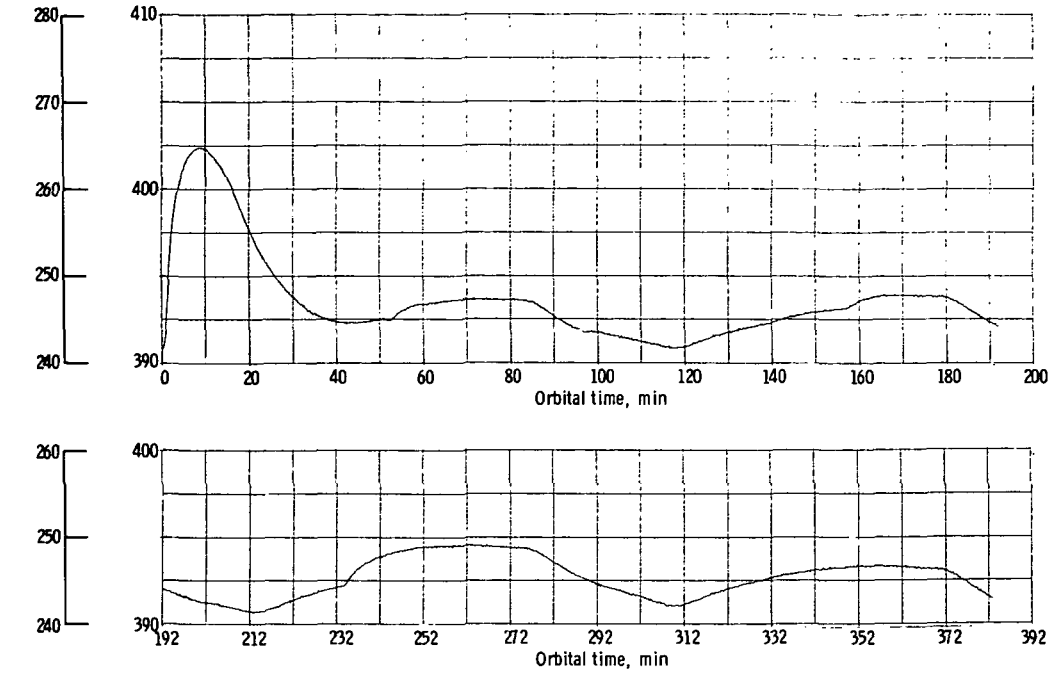

(a) On high-temperature-radiator fluid inlet temperature.

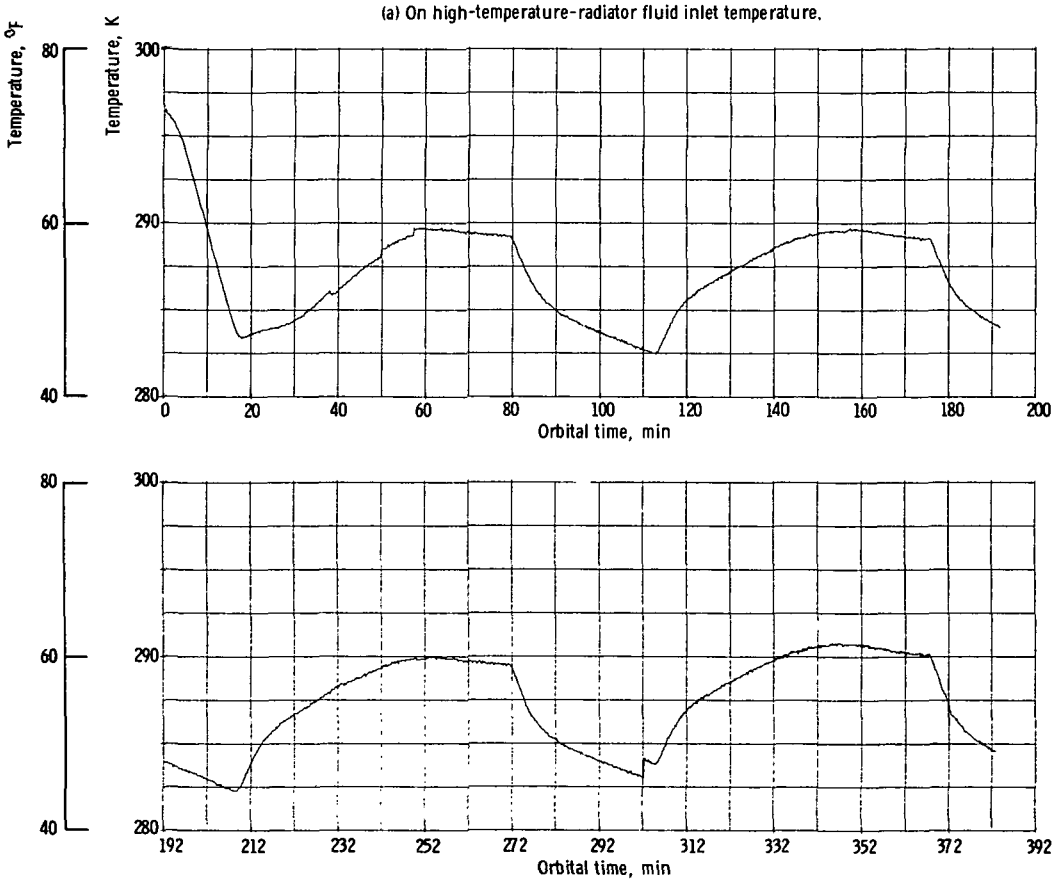

(b) On radiator outlet temperature.

Figure 28. - Effect of engine operation at constant compressor discharge pressure and constant heat-source power on high-temperature-radiator fluid inlet temperature and on radiator outlet temperature as functions of orbital time.

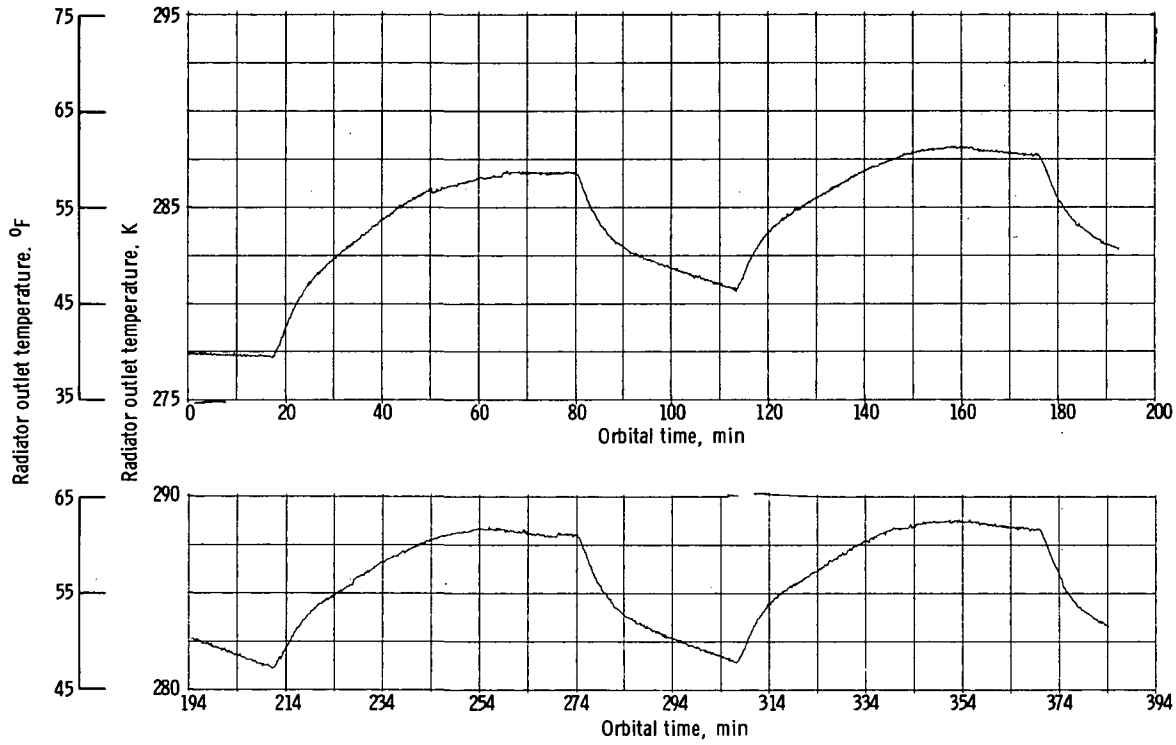

Figure 29. - Effect of engine operation at constant gas inventory and constant turbine inlet temperature - transient started in steady state and with bypass doors closed - on radiator outlet temperature as function of orbital time.

NASA-Langley, 1974 E-7716

NATIONAL AERONAUTICS AND SPACE ADMINISTRATION
WASHINGTON, D.C. 20546

OFFICIAL BUSINESS
PENALTY FOR PRIVATE USE $300

SPECIAL FOURTH-CLASS RATE BOOK

POSTAGE AND FEES PAID
NATIONAL AERONAUTICS AND SPACE ADMINISTRATION
451

U.S.MAIL

POSTMASTER: If Undeliverable (Section 158 Postal Manual) Do Not Return

"The aeronautical and space activities of the United States shall be conducted so as to contribute . . . to the expansion of human knowledge of phenomena in the atmosphere and space. The Administration shall provide for the widest practicable and appropriate dissemination of information concerning its activities and the results thereof."

—NATIONAL AERONAUTICS AND SPACE ACT OF 1958

NASA SCIENTIFIC AND TECHNICAL PUBLICATIONS

TECHNICAL REPORTS: Scientific and technical information considered important, complete, and a lasting contribution to existing knowledge.

TECHNICAL NOTES: Information less broad in scope but nevertheless of importance as a contribution to existing knowledge.

TECHNICAL MEMORANDUMS: Information receiving limited distribution because of preliminary data, security classification, or other reasons. Also includes conference proceedings with either limited or unlimited distribution.

CONTRACTOR REPORTS: Scientific and technical information generated under a NASA contract or grant and considered an important contribution to existing knowledge.

TECHNICAL TRANSLATIONS: Information published in a foreign language considered to merit NASA distribution in English.

SPECIAL PUBLICATIONS: Information derived from or of value to NASA activities. Publications include final reports of major projects, monographs, data compilations, handbooks, sourcebooks, and special bibliographies.

TECHNOLOGY UTILIZATION PUBLICATIONS: Information on technology used by NASA that may be of particular interest in commercial and other non-aerospace applications. Publications include Tech Briefs, Technology Utilization Reports and Technology Surveys.

Details on the availability of these publications may be obtained from:

SCIENTIFIC AND TECHNICAL INFORMATION OFFICE

NATIONAL AERONAUTICS AND SPACE ADMINISTRATION

Washington, D.C. 20546

NATIONAL AERONAUTICS AND SPACE ADMINISTRATION
WASHINGTON, D.C. 20546

OFFICIAL BUSINESS
PENALTY FOR PRIVATE USE $300

SPECIAL FOURTH-CLASS RATE BOOK

POSTAGE AND FEES PAID
NATIONAL AERONAUTICS AND SPACE ADMINISTRATION
451

U.S.MAIL

POSTMASTER: If Undeliverable (Section 158 Postal Manual) Do Not Return

"The aeronautical and space activities of the United States shall be conducted so as to contribute . . . to the expansion of human knowledge of phenomena in the atmosphere and space. The Administration shall provide for the widest practicable and appropriate dissemination of information concerning its activities and the results thereof."

—NATIONAL AERONAUTICS AND SPACE ACT OF 1958

NASA SCIENTIFIC AND TECHNICAL PUBLICATIONS

TECHNICAL REPORTS: Scientific and technical information considered important, complete, and a lasting contribution to existing knowledge.

TECHNICAL NOTES: Information less broad in scope but nevertheless of importance as a contribution to existing knowledge.

TECHNICAL MEMORANDUMS: Information receiving limited distribution because of preliminary data, security classification, or other reasons. Also includes conference proceedings with either limited or unlimited distribution.

CONTRACTOR REPORTS: Scientific and technical information generated under a NASA contract or grant and considered an important contribution to existing knowledge.

TECHNICAL TRANSLATIONS: Information published in a foreign language considered to merit NASA distribution in English.

SPECIAL PUBLICATIONS: Information derived from or of value to NASA activities. Publications include final reports of major projects, monographs, data compilations, handbooks, sourcebooks, and special bibliographies.

TECHNOLOGY UTILIZATION PUBLICATIONS: Information on technology used by NASA that may be of particular interest in commercial and other non-aerospace applications. Publications include Tech Briefs, Technology Utilization Reports and Technology Surveys.

Details on the availability of these publications may be obtained from:

SCIENTIFIC AND TECHNICAL INFORMATION OFFICE

NATIONAL AERONAUTICS AND SPACE ADMINISTRATION

Washington, D.C. 20546